Université d'Ottawa · University of Ottawa

Direct Current Resistance Measurement Structure for Determining Line Width and Metal Thickness Variations in Surface Acoustic Wave Devices

By

© Bruce Calder

Thesis submitted to the

Faculty of Graduate Studies and Research

In partial fulfillment of the requirements

Of the Master of Science in Physics

Department of Physics

University of Ottawa

150 Louis Pasteur

Ottawa, Ontario

K1N 6N5

0-612-36672-3

Abstract

SAW devices are often designed to act as bandpass filters. The electrical properties of surface acoustic wave (SAW) devices are difficult to measure prior to being wirebonded into packages. Matching difference in SAW devices cause difficulties in obtaining accurate measurement of the centre frequency of the bandpass reponse of unpackaged SAW devices. The variation in centre frequency of SAW devices due to fabrication variation is dependent on the variation of the width and thickness of the metal fingers of the SAW device.

The width and thickness of aluminum lines of a surface acoustic wave device can be determined by direct current resistance measurement of a single thickness, two part aluminum structure. The first component is based on the van der Pauw sheet resistance structure. The second component is a direct current line width measurement structure.

The direct current resistance structure presented here provides a method for determining the width and thickness of the fingers of the interdigital transducer of a SAW device. From the width and thickness information, the centre frequency and bandwidth of a SAW device can be extrapolated.

Both direct current and radio frequency measurements can be made rapidly and reproducibly with the aid of computer automation. An automated system for each type of measurement (direct current and radio frequency) will also be described here.

A seminar on this topic was presented on May 7, 1998 at the University of Ottawa.

The author has worked in semiconductor lasers and GaAs MESFETs. He is now working as a product engineer for Nortel on Surface Acoustic Wave devices and GaAs Hetero-junction Bi-polar Transistor circuits.

The author received the Nortel Award of Merit for Innovation for the design and construction of the automated SAW die testing system described in this paper.

The author would like to thank Nortel for the use of its resources. In particular, the author would like to thank Dr. Zhuo-hui Chen, Steve Beaudin, and Daniel Duguay; for their technical advice. Robert Arnold for the original concept and design of the DCRMS. Thanks to Dr. Fortin for his guidance and patience. Annie Jacobs for her technical drawings. Andrea Morelli for contributions on the experimental work. Most importantly, the author would like to thank Patricia Mcallister for her time, patience, proof reading, and contributions to this thesis.

Thanks to the all the people at Nortel Microwave Modules for all of their help and encouragement.

1.0 Plan of Thesis

2.0 Introduction

2.1 Background

Acoustic waves in solids propagate at velocities five orders of magnitude less than electromagnetic waves. The appeal of surface acoustic waves (SAWs) is the confinement of acoustic energy near the surface of a solid where it can be tapped or modified while propagating. With the invention of the interdigital transducer (IDT), the ability to generate SAWs from electromagnetic signals and electromagnetic signals from SAWs was created. This invention led to the capability of processing high frequency signals with relatively simple passive components.

There are many articles featuring the current applications of SAW devices[1]. Every television set produced today contains at least one SAW filter which is used in the intermediate frequency (IF) stage of the receiver[2]. Satellite receivers contain SAW filters at centre frequencies varying from 400 to 500 MHz.[3] SAW devices are also used in digital mobile telephone systems as IF filters. For wireless radio frequency (RF) purposes, SAW devices are used as bandpass filters in the 450 MHz to 2 GHz range.

---

[1] **L.A. Coldren, R.L. Rosenberg. SAW resonator filter overview: Design and performance tradeoffs. *1978 Ultrasonics Symposium Proceedings*, IEEE Cat. #78CH 1344-1SU, pp. 422-432.**

[2] **C. Ruppel, R. Dill, A. Fisherauer, G. Fisheraurer, W. Gawlik, J. Machui, F. Muller, L. Reindl, W. Ruile, G. Scholl, I. Schropp, K. Wagner. SAW devices for consumer communication applications. *IEEE Transactions on Ultrasonics, Ferroelectrics, and Frequency Control*, 2 Sept (1993), pp. 438-451.**

[3] **C. Ruppel, R. Dill, A. Fisherauer, G. Fisheraurer, W. Gawlik, J. Machui, F. Muller, L. Reindl, W. Ruile, G. Scholl, I. Schropp, K. Wagner. SAW devices for consumer communication applications. *IEEE Transactions on Ultrasonics, Ferroelectrics, and Frequency Control*, 2 Sept (1993), pp. 438-451.**

With the surge in growth of the wireless communication industry, the demand for SAW devices is increasing.

SAW devices are attractive for many reasons:

(a) They operate most readily in the frequency range from around 10 MHz to well over 1 GHz and so fill a gap between 'natural' regimes of lumped component and microwave technologies. SAW bandwidths range from a few tens of kHz to more than 500 MHz.

(b) In a SAW device the signal is concentrated at the substrate surface and is therefore readily available to be tapped, guided, reflected, focused, absorbed, etc. This leads to an extremely wide design flexibility and a large spectrum of applications.

(c) SAW device fabrication exploits the techniques of photolithography developed by the semiconductor industry. Performance characteristics are determined by the single photolithographic pattern and the properties of the single crystal substrate. Therefore reproducibility is good. Since only a single surface of the substrate is used, the under side of the substrate can be rigidly attached. Thus SAW devices are rugged and reliable.[4]

(d) SAW devices are relatively cheap compared to the corresponding active devices made using silicon or GaAs technology.

(e) The response frequency of the SAW can be changed after fabrication

---

[4] **F. Ananasso. Review of SAW devices and their signal processing applications in space communications, *International Journal of Satellite Communications*, 7 (1989), pp. 235-261.**

using etching of the piezoelectric substrate or of the metal fingers.

Most of this thesis concerns itself with the particularities of reason (c): the characteristics of photolithographic and metal deposition techniques developed by the semiconductor industry.

2.2 Fabrication and Testing

Even with the relative simplicity of manufacture of the single metal layer SAW device, the manufacturability of SAW devices suffers from difficulty in measuring the radio frequency (RF) properties of the devices. Contact probing of the SAW devices is difficult to conduct accurately due to electrical mismatches between the testing equipment and the SAW devices; and limitations of the probe tip configuration with respect to the final wire bond locations. Without custom construction probe tips for each new SAW device layout, it is difficult to test a bare SAW die in the same manner as a packaged die. The measured frequency response of a SAW device prior to and following wire bonding differs significantly. Three major causes of this difference in response are impedance matching, pad layout, and stress imposed during the die attachment process.

Without the proper impedance match, SAW devices do not necessarily operate as well as they do properly matched. Improper impedance matches can lead to reflection between the fingers, thus distorting the measured signal. An improperly matched SAW device has its transmission signal (power versus frequency) distorted from a regular rectangular shape to a less regular shape.

The pad layout of a device can make it difficult to conduct a standard four probe tip (two sets of probes, each with a ground tip and a signal tip) or six probe tip (two sets of probes, each with a grounded tip, a signal tip, and a second ground tip) measurement. Another problem is that some bond pad layouts may make it impossible to ground all the ground pads of the SAW device. This may not allow easy probing of a SAW device without constructing custom probe tip arrangements. A full probe card with RF probes can cost upwards of $3000 US.

Stress affects the crystal structure of the device. Changes in stress (epoxy die attachment) can cause strain in the crystal structure of the device and therefore change the surface velocity of the SAW. A change in surface velocity induces a change in the frequency response of the SAW device.

The ratio of the amplitude of the output signal from a SAW device to the amplitude of the input signal is difficult to measure. This makes it difficult to measure a consistent centre frequency or bandwidth for a SAW device. A properly designed, packaged, and matched SAW device has very little variation in the ratio of output signal to input signal over the range of the pass band. On the other hand, an unpackaged, unmatched SAW device often produces a response with significant variation in this ratio over the frequency range of the pass band of the SAW device. This variation, or ripple, over the pass band makes it very difficult to measure key bandpass filter characteristics such as centre frequency and bandwidth.

If a SAW device cannot be accurately measured immediately after fabrication, the manufacturer will have to wait and undergo the expense of packaging the devices before he will know whether the parts are within specifications. If these devices could be measured before packaging, the unnecessary expense of packaging faulty parts could be avoided and fabrication difficulties leading to the creation of flawed parts could be identified and dealt with earlier in the process.

2.3 Mass Loading

The variation in centre frequency between SAW devices of the same design and fabrication process stem from the variation in the width and thickness of the metal fingers of the IDT. When a SAW device is fabricated, its frequency can vary by as much as 150 ppm due to manufacturing variations. The variation in the width and thickness of the metal fingers of the IDT originated from the imperfect control of the fabrication process. Imperfect as they are, developments in semiconductor processing have enabled the fabrication of SAW devices with extremely tight physical tolerances (and ensuing tight electrical tolerances).

Changing the height of the aluminum electrodes with respect to the surface of the quartz will shift the frequency of the device.[5] The mass of the metal fingers is directly proportional to their width and thickness. It is the mass of fingers, in the form of mass loading, that changes the velocity of the SAW. Variation in the velocity of the SAW changes the centre frequency of the bandpass response of the SAW device. Since the SAW is only affected by mass changes along its direction of propagation, mass variation perpendicular to the direction of propagation, such as the length of the fingers of the IDT, has no effect on the SAW.

---

[5] **J. Browne. SAW devices set long-term stability marks, *Microwaves and RF*, May (1994), pp. 136-138.**

Mass loading is defined as[6]

> The change in phase velocity of a SAW produced by a thin layer on the substrate of higher density than that of the substrate; perturbations in reflection, velocity, and dispersion that occur due to loading effects of thin films on the substrate surface.

In many publications, the concerns with mechanical or mass loading revolve around distortion of the frequency response of the SAW device.[7] Here we will be more interested in the perturbation in velocity of the SAW.

In quartz substrates the relationship between the change in mass of the metal fingers and the change in velocity of the SAW is linear. By measuring the width and thickness of the metal fingers, and therefore the mass, the centre frequency of a SAW device can be determined.

The width and thickness of the metal fingers can be measured using optical and mechanical methods, but the cost, time, and effort of obtaining these measurements makes them impractical in a manufacturing environment. For small metal thickness and line widths there are concerns about the accuracy of these measurement tools.

2.4 Direct Current Resistance Measurement Structure (DCRMS)

A DCRMS based on the van der Pauw resistance structure was developed by

---

[6] **E. Mariani. Terms and definitions for surface acoustic wave devices. *IEEE Transactions on Sonics and Ultrasonics*, 4, July (1985), pp. 476-481.**

[7] **D. P. Morgan. Surface-Wave Devices for Signal Processing. Elsevier Sceince Publishing, 1985.**

Robert Arnold.[8] The structure consists of two components, a van der Pauw sheet resistance structure (SRS) (Figure 1) from which the metal thickness can be determined, and a line width (or bridging) measurement structure (LWS) (Figure 2) with which variation of the line width can be measured. Both of the components of the DCRMS operate on the basis that a change in resistance of either component means an inversely proportional change in the thickness or width of the metal lines of the metal lines of SAW devices fabricated on the same wafer.

The DCRMS and the SAW devices are formed from a single uniform layer of deposited metal using fabrication techniques designed by the semiconductor circuit industry. Since the DCRMS and the SAW devices are fabricated on the same wafer, using the same techniques, and at the same time; process variations affecting the SAW device should affect the DCRMS. Under this assumption, the DCRMS is to be used to determine variations in SAW devices.

---

[8] **R. Arnold. SAW Test Insert Guide. Internal Nortel Publication, Oct. (1996).**

Figure 1 (Basic Sketch of the van der Pauw Sheet Resistance Structure)

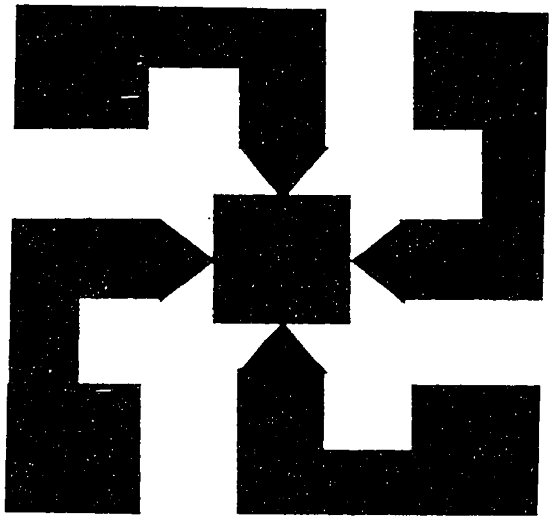

Figure 2 (Basic Sketch of a Line Width or Bridging Structure)

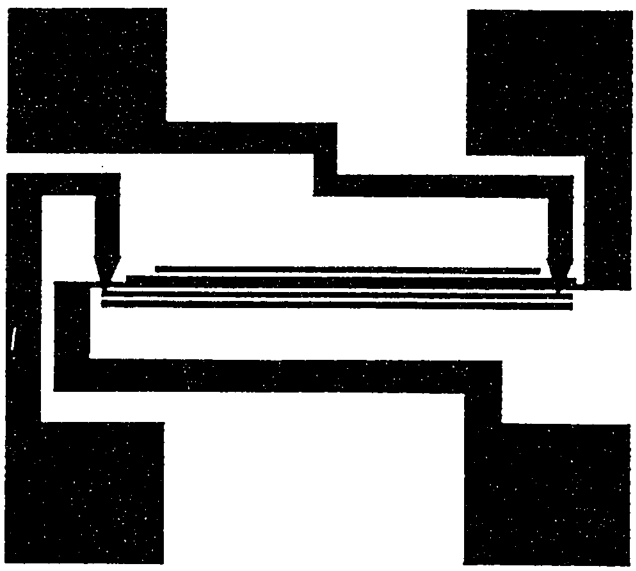

By making simple dc resistance measurements, variations in line thickness and width can be monitored. Compared to optical and mechanical measurement techniques, dc resistance measurements can be made with relatively inexpensive equipment. With the help of computer automation, dc measurements can be made in relatively short periods of time.

The exact description of the DCRMS and its component structures can be found in section 3.4.

3.0 Theory

3.1 Rayleigh Waves and the Piezoelectric Effect

A surface acoustic wave, sometimes known as a Rayleigh wave, is non-dispersive and has displacements which decay exponentially away from the surface so that most of the energy is confined within a depth equal to one wavelength.[9] The energy of the components of the first mode of a Rayleigh wave are shown in Figure 3. The wave is strongly confined, with typically 90% of the energy propagating within one wavelength of the surface.[10] The wave has displacement components in the u_1 direction of propagation (x_1) and u_3 perpendicular to the surface (x_3), but the wave has no energy component u_2 on the surface perpendicular to the direction of propagation (x_2).

Figure 3 (Displacement of a Rayleigh Wave)

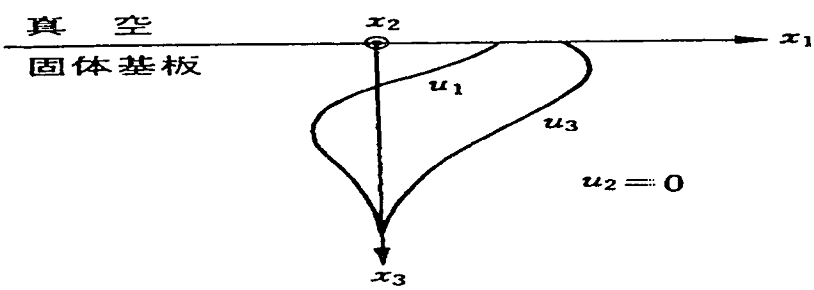

The velocity of a surface acoustic wave in quartz is near 3000 ms^{-1} depending on

---

9 **D. P. Morgan. Surface acoustic wave devices and applications, *Ultrasonics*, 11 (1973), pp. 121-131.**

10 **D. P. Morgan. Surface-Wave Devices for Signal Processing. Elsevier Sceince Publishing, 1985.**

the cut of the quartz.

Figure 4[11] is representative of particle motion under the action of a SAW. The top row indicates particle motion at the surface of the solid. Note that the particles have less range of motion the farther they are away from the surface. The third row of particle has no x_1 motion. This is representative of u_1 being 0 at that point.

Figure 4 (Motion of Particle in a Surface Acoustic Wave)

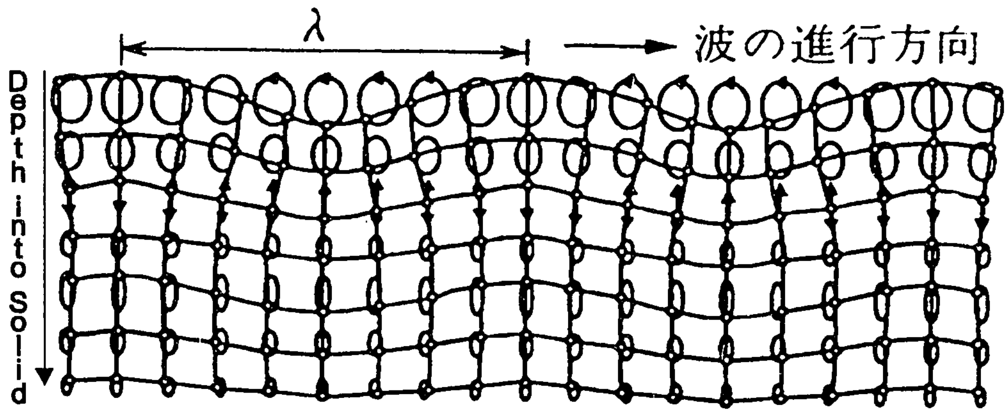

When a single crystal piezoelectric material is placed in an electric field, the crystal exhibits tensile and compressive strain (Figure 5). Conversely, when a piezoelectric single crystal is strained, electric charges appear on the surface of the material. This is called the direct piezoelectric effect.

---

[11] **Handbook of Elastic Wave Device Technology. Elastic Wave Device Technology Committee. #150, p. 56. (Translated from Japanese)**

Figure 5 (Direct Piezoelectric Effect) [12]

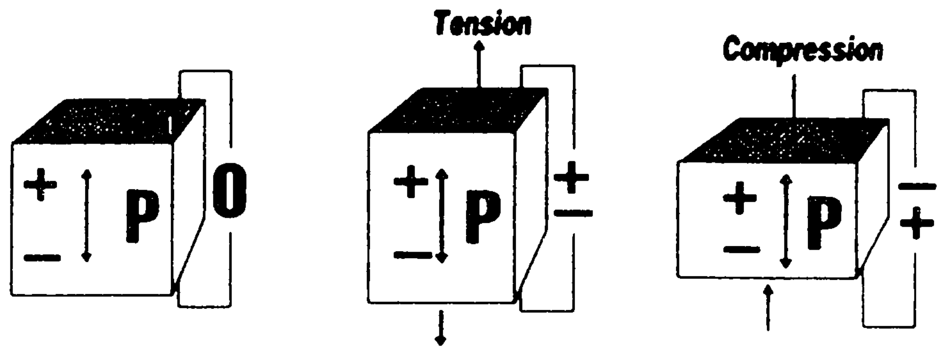

Figure 6 (Interdigital Transducer) [13]

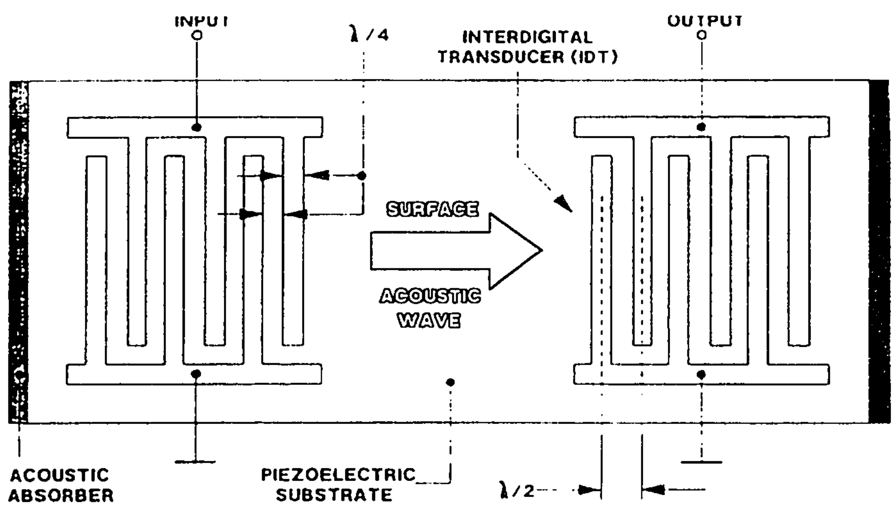

An RF signal applied to an IDT causes compressions and expansions on the substrate surface, which produces a traveling piezoelectric wave from the input to the

[12] Valpey-Fischer Corporation. Piezoelectric transducer crystals. Crystal specifications.

[13] F. Ananasso. Review of SAW devices and their signal processing applications in space communications, *International Journal of Satellite Communications*, 7 (1989), pp. 235-261.

output IDT, where the piezoelectric oscillations are converted back into an RF signal (Figure 6).[14]

When an oscillating voltage is applied, the transducer generates an electric field, which is spatially periodic, with period, L, equal to the spacing of the electrodes connected to one of the bus-bars. Owing to the piezoelectric effect, a corresponding pattern of mechanical displacements is also produced. Efficient coupling to surface waves occurs if the transducer period L is equal to or close to the surface-wave wavelength for a given frequency.[15]

3.2 Transmission Measurements of Surface Acoustic Wave Devices

A frequency response of a bandpass SAW device is shown in Figure 8a. Figure 8a shows a graph of S21 amplitude versus frequency. S21 amplitude is the ratio of the amplitude of the signal received by port 2 over the amplitude of the signal outputted by port 1 (in dB). Port 1 and port 2 of the network analyzer are shown in Figure 7. In testing, the SAW device is wired between port 1 and port 2. The signal is outputted by port 1, passes through the SAW device, and is received by port 2. The resulting S21 amplitude is the relative amplitude of the signal transmitted through the device.

---

[14] **F. Ananasso. Review of SAW devices and their signal processing applications in space communications, *International Journal of Satellite Communications*, 7 (1989), pp. 235-261.**

[15] **D. P. Morgan. Surface-Wave Devices for Signal Processing. Elsevier Sceince Publishing, 1985.**

Figure 7 (HP8753C Network Analyzer)

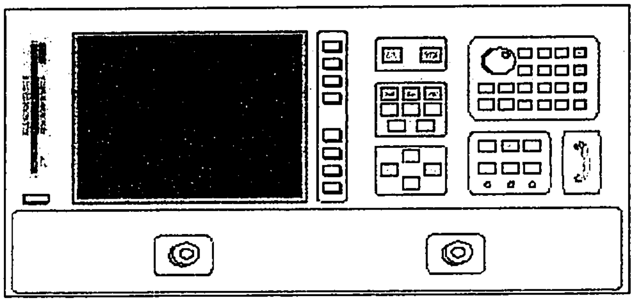

Port 1 **Port 2**

Figure 8a (Typical Shape of S21 Transmission Response of a SAW Device)

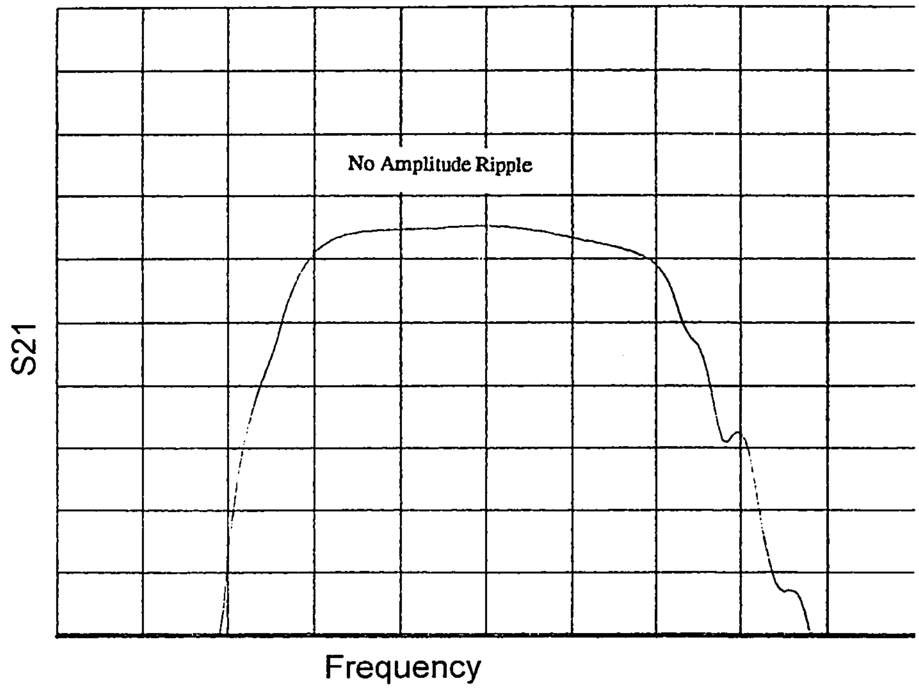

The centre frequency of the bandpass is dependent at which dB the measurement was conducted. For example, the centre frequency at -3dB corresponds to the point midway between the two points -3dB from the peak point of the bandpass response (the point of minimum insertion loss). The sides of a bandpass response generally have different slopes, so the centre frequency varies with dB. With unmatched, unpackaged SAW devices, the bandpass shape can have so much ripple that there is no obvious peak point from which to measure the centre frequency (Figure 8b).

Figure 8b (Typical Shape of an Unmatched S21 Transmission Response of a SAW Device)

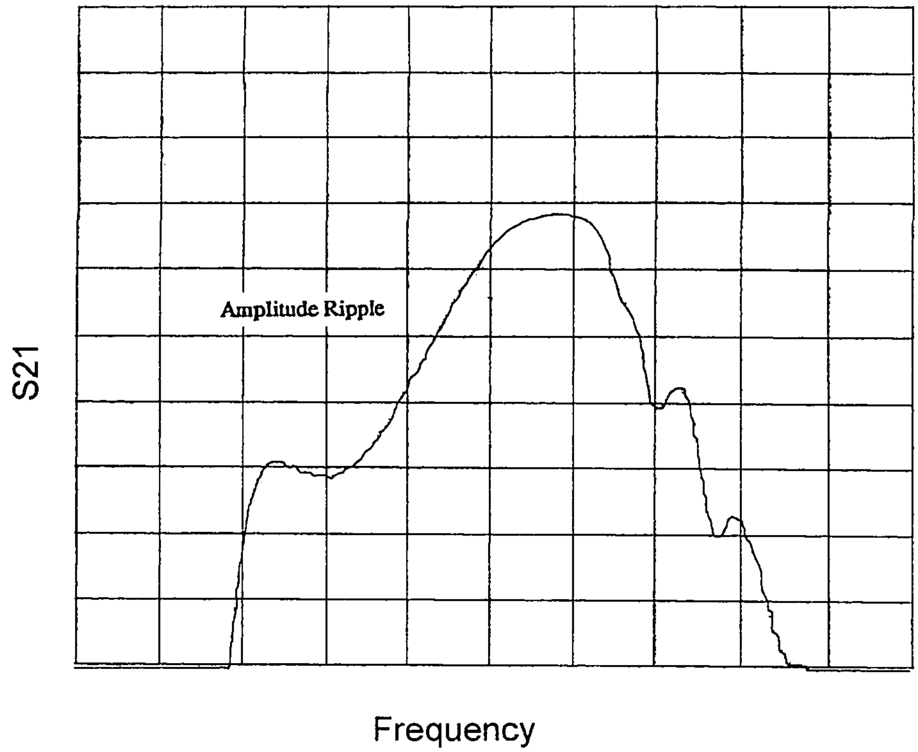

A first order approximation of the centre frequency is dependent only on the period, Λ, of the electrodes. The centre frequency is also affected by the second order effects of mass loading and electrical loading. The very thin layer of metal acting as a transducer has the effect of reducing the wave velocity because of the change in electrical boundary conditions. This phenomenon is called electrical loading. However, for weakly piezoelectric material such as quartz, the effects of electrical loading are negligible.

3.3 Mass Loading

Mass loading is dependent on the mass of the thin film fingers of the IDT. Aluminum fingers of IDTs are generally between 200 A to 10000 A in thickness and 0.5μμ to 10μμ in width.

For the theory of massloading, the coordinate system is chosen such that x (also shown as x_1) indicates the direction of wave propagation and z (also shown as x_3) indicates the direction into the substrate perpendicular to the direction of propagation as shown in Figure 9. The length of the metal lines is much longer than the width of the line. Therefore, the Rayleigh Wave amplitude is independant of y (x_2 in Figure 3).

Figure 9 (Coordinate System for Rayleigh Wave Theory) [16]

(Metal lines on a piezoelectric substrate. SAW propagating in the direction x.)

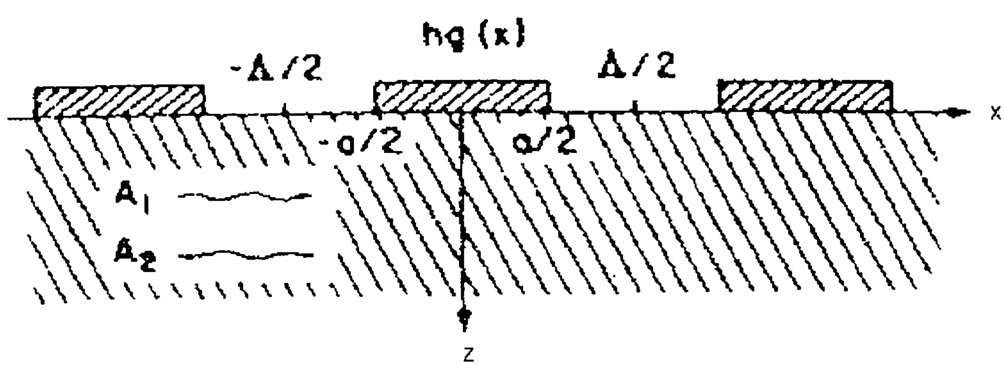

[16] D. Chen, H. A. Haus. Analysis of Metal-Strip SAW Gratings and Transducers, *IEEE Transactions on Sonics and Ultrasonics*, 12 (1985), pp. 395-408.

In Figure 9, a is the width of the metal line, h is the maximum height of the metal line, and Λ is the period of the lines. A_1 is the acoustic wave in the direction of propagation. A_2 is the reflected acoustic wave. The direction of propagation is x and z in the coordinate perpendicular to x and into the material.

The shape of the metal line is described by the function h * g(x) where $g_{max} - g_{min} = 1$.

The unperturbed Rayleigh wave displacement on the equivalent isotropic medium is[17]:

$$U_x = (e^{-rk_R z} - \frac{1+q^2}{2} e^{-qk_R z}) e^{-j(s+N)\theta} \qquad (1)$$

$$U_y = j(-re^{-rk_R z} + \frac{1+q^2}{2q} e^{-qk_R z}) e^{-j(s+N)\theta} \qquad (2)$$

where r and q are normalized functions of the Poisson ratio ν. ν is equal to the strain caused by the lateral compression over the strain caused by the longitudinal distortion. The dimensionless variable θ and the wave numbers s and N are defined by

[17] **I. A. Victorov. <u>Rayleigh and Lambda Waves</u>. Plenum, 1967.**

$$\theta = \frac{2\pi x}{\lambda} \qquad (3)$$

$$(s+N) = \frac{k_R \Lambda}{2\pi} \qquad (4)$$

where s is limited to the range $0 < s < 1$, N is an integer, λ is the wavelength of the SAW, Λ is the period of the metal lines, and k is the propagation wavenumber of the SAW.

The quasistatic electrostatic potential, Φ, has the boundary conditions

$$\Phi_{continuous}, \frac{a}{2} < |x| < \frac{\Lambda}{2} \qquad (5)$$

$$\Phi = 0, |x| < \frac{a}{2} \qquad (6)$$

A full equation for the electrostatic potential can be found in Reference[18]. The equation of motion for a SAW is[19]

---

[18] **S. Datta and B.J. Husinger. "First-Order Reflection coefficient of surface acoustic waves from thin-strip overlays". J. Appl. Phys., vol 51, no. 9, pp. 4817-4823.**

[19] **B. A. Auld. Acoustic Fields and Waves in Solids. John Wiley, 1, 1973, pp. 298-300.**

$$\omega^2 \int dv \rho u_i^* u_i = \int dv (\frac{\partial u_i^*}{\partial x_j} c_{ijkl} \frac{\partial u_k}{\partial x_l} + \frac{\partial u_i^*}{\partial x_j} e_{ijk} \frac{\partial \Phi}{\partial x_k} + \frac{\partial \Phi^*}{\partial x_i} e_{ijk} \frac{\partial u_j}{\partial x_k} + \frac{\partial \Phi^*}{\partial x_i} e_{ij} \frac{\partial \Phi}{\partial x_j}) \quad (7)$$

Where u_i , u_j , and u_k are the components of the wave displacements in the directions x_i , x_j, and x_k; x has the periodic boundary condition x = +- l with very large l compared to Λ; c_{ijkl} is the elasticity tensor symmetric in directions ij and kl respectively; e_{ijk} is the piezoelectric tensor symmetric in jk; v is the Rayleigh velocity. From Equation 8 and Chen et al.[20], the velocity shift of the SAW simplifies to two components: a velocity shift component due to mechanical contributions (stress and mass loading) and an electrical component.

The mechanical component of the velocity shift is dependant on the metal and the substrate. For a particular metal line on a particular substrate at a specific metallization ratio, the mechanical contribution to the velocity shift is a constant multiplied by (h/λ). The electrical component of the velocity shift is approximately zero for quartz[21]. Therefore the velocity shift ($\Delta v/v_R$) (v is velocity, υ is frequency) is dependent on the thickness of the metal divided by wavelength of the SAW (λ).

$$\frac{\Delta v}{v_R} = (\frac{\Delta v}{v_R})_m (\frac{h}{\lambda}) + (\frac{\Delta v}{v_R})_e \quad (8)$$

The mass loading component, $(\Delta v/v_R)_m$ is proportional to the inverse of the period and is a function of the shape of the metal line.

---

[20] **D. Chen, H. A. Haus. Analysis of Metal-Strip SAW Gratings and Transducers, *IEEE Transactions on Sonics and Ultrasonics*, 12 (1985), pp. 395-408.**

[21] **D. Chen, H. A. Haus. Analysis of Metal-Strip SAW Gratings and Transducers, *IEEE Transactions on Sonics and Ultrasonics*, 12 (1985), pp. 395-408.**

$$\left(\frac{\Delta v}{v_R}\right)_m \propto \frac{1}{\Lambda}\int_{-\pi}^{\pi} g(\theta)d\theta \qquad (9)$$

The function g(θ) is the shape of the metal line, where θ is defined in (3). The function g(θ) can be rewritten as g(x),

$$\int_{-\pi}^{\pi} g(\theta)d\theta = \int_{-\Lambda/2}^{\Lambda/2} g(x)dx \qquad (10)$$

where g(x) is the shape of the line over one period Λ. Since $g_{max} - g_{min} = 1$ (see above) and the line can be approximated as being a perfect rectangle, the function g(x) = 1 from –a/2 to a/2 and g(x) = 0 outside of that range.

$$\int_{-\Lambda/2}^{\Lambda/2} g(x)dx = \int_{-a/2}^{a/2} dx = a \qquad (11)$$

Therefore

$$\left(\frac{\Delta v}{v_R}\right)_m \propto \frac{a}{\Lambda} \qquad (12)$$

For a particular SAW device, the period, Λ, remains constant, so:

$$\frac{\Delta v}{v_R} \propto a(\frac{h}{\lambda}) \qquad (13)$$

From this, the variation in the centre frequency for a SAW device is dependant on the variation in the mass (which varies with height and width) of the metal lines.

3.4 Characteristic Impedance and Bandwidth

Velocity changes at surface discontinuities (unmetallized to metallized surfaces) will also be accompanied by changes in equivalent electrical impedance.[22] For a transducer to transducer SAW device, a change in the match of the device cause reflections of the SAW by the metal lines. For an optimal SAW device, the reflections caused by the metal lines is zero.

The downside to this reflection is that it will cause triple transit interference.[23] Triple transit refers to the SAW travelling from the input IDT to the output IDT. The SAW is reflected by the output IDT back to the input IDT. Part of this signal is reflected again by the input IDT. The SAW travels once more from the input IDT to the output IDT. Part of that triple transit signal is transmitted. The SAW will have made three transits of the gap between the input and output IDTs (and five, seven, nine .... with decreasing amplitude following each reflection).

This triple transit signal is smaller than the original single transit signal. The difference is that the triple transit signal arrives 2τ after the main signal, where τ is the time it takes for the SAW to travel from the input IDT to the output IDT. This

---

[22] **Colin Campbell. Surface Acoustic Wave Devices and Their Signal Processing Applications. Academic Press Inc. 1989, p. 106.**

interference will cause amplitude ripple in the transmitted signal.

Amplitude ripple is defined as the maximum peak to peak difference in amplitude of the pass band of the transmitted signal. In general, SAW devices are designed with a mismatch between the input and output IDT. For a well designed SAW device, variation in impedance should only cause small changes in amplitude ripple. In this paper, changes in amplitude ripple will manifest itself as a variation in bandwidth. When the amplitude ripple changes, the measured bandwidth will change.

Characteristic impedance is defined as:

$$Z_o = \sqrt{L/C} \qquad (14)$$

where L in the distributed series inductance / unit length of the IDT and C is the distributed shunt capacitance / unit length of the IDT.

The frequency, υ, is given as

$$\nu = \frac{1}{\sqrt{LC}} \qquad (15)$$

Putting equations (14) and (15) together, the inductance term is eliminated.

$$Z_o = \frac{1}{\nu C} \qquad (16)$$

[23] **Colin Campbell. <u>Surface Acoustic Wave Devices and Their Signal Processing Applications</u>. Academic Press Inc. 1989, p. 66.**

The capacitance C is defined for an electrode pair SAW device as:

$$C = C_o NW \qquad (17)$$

where N is the number of finger pairs in the SAW device, W is the width of the SAW device aperture (length of the metal line), and C_o is the capacitance / finger pair / unit length. N and W will not vary in a given SAW.

C_o is dependant on the substrate and the metalization ratio η.

$$\eta = \frac{a}{\Lambda} \qquad (18)$$

The mechanical and electrical properties of the substrate vary negligibly and can be assumed to be constant. Therefore the capacitance is only dependant on the metalization ratio.

Ritchie et al.[24] present a numerical analysis of the relationship between capacitance and metalization ratio. For a metalization ratio near 0.5, the relationship between capacitance and metalization ratio can be assumed to be linear for very small variation in the latter. Since this thesis deals with variations in metalization ratio of under 2% (from a metalization ratio of 0.5), the characteristic impedance is:

---

[24] S. M. Ritchie, B.P. Abbott and D.C. Malocha, "Description and development of a Saw filter CAD system," *IEEE Trans. Microwave Theory & Techniques*, Vol. 36, pp. 456-466, 1981.

$$Z_o \propto \frac{1}{v\eta} \qquad (19)$$

From (19), it can be seen that the the matching is dependant on the metalization ratio and variation in the velocity of the SAW. From this, the variation in the line width (metalization ratio) should be the principal factor in impedance changes. However, since mass loading has an effect on surface velocity, the thickness of the metal lines should also affect impedance.

The impedance changes will be measured by changes in bandwidth. For extremely small changes in impedance, the bandwidth will also vary by a small amount. The intention is to use the DCRMS to monitor variation in line width. If there is a linear relationship between bandwidth and line width for very small perturbations of line width, then the resulting variation in bandwidth of the SAW may be determined by measuring variations in the line width.

3.5 Direct Current Resistance Measurement Structure

The DCRMS is a patterned single layer of deposited metal laid out on the surface of a piezoelectric substrate. The pattern, itself, is a single lithographic mask plate.

The DCRMS pattern is made up of two components: a sheet resistance module and a line width module. The sheet resistance component is based on the van der Pauw sheet resistance structure.[25] The van der Pauw sheet resistance structures and bridge

---

[25] **L. J. van der Pauw, *Phillips Tech. Rev.*, 20 (1958), p. 220.**

structures (similar to the line width structures (LWS) of the DCRMS) are used in the silicon industry to measure sheet resistance and line width of diffused or implanted conducting areas.[26] A diagram of the DCRMS is given in Figure 10. The basic DCRMS design originates from two structures designed by Prometrix for lithographic analysis.[27]

[26] **M. G. Buehler, S. D. Grant, W. R. Thurbar. Bridge and van der Pauw sheet resistors for characterizing the line width of conducting layers.** ***J. Electrochem Soc.: Solid-State Science and Tech.***, **April (1978), pp. 650-654.**

[27] **Prometrix LithoMap LM25 Applications Manual. Feb. 1987.**

Figure 10 (Layout of the Lithographic Pattern of the DCRMS)

(The LWSs are identified by the width of the measurement line of the structure. Ie. the 5 micron LWS has a measurement line 5 micron in width. The structure in the centre of the LWSs is the SRS)

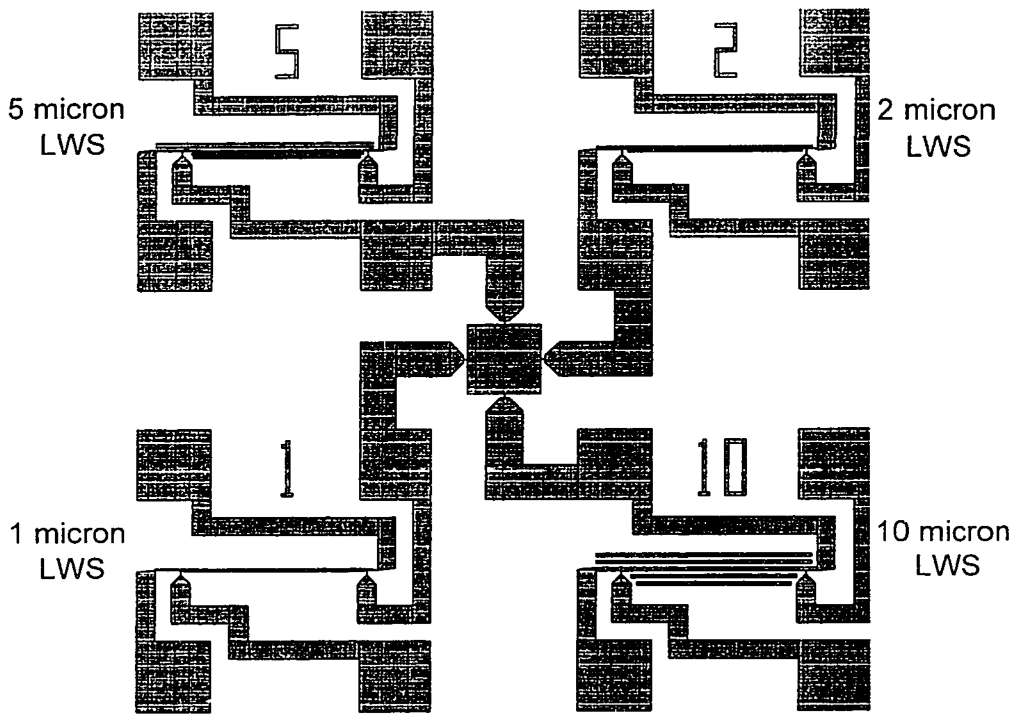

Centre Structure - SRS

The DCRMS is composed of five individual components: a sheet resistance structure (SRS) and four line width resistance structures (LWSs). The line width module is constructed with four different line widths: 1µm, 2µm, 5µm, and 10µm; to allow monitoring line width variation in SAW devices with different widths of fingers. The line to be measured in each structure is the centre of the five lines on a LWS. The five lines are easiest to see in the 10 μm LWS. The structure is designed to be used in determining variation in finger width for SAW devices with finger width from 1μm to 10um. The DCRMS is 2mm by 2mm in surface area.

The idea behind the DCRMS is that it will undergo the same processing conditions as a SAW device on the same quartz wafer. The SAW devices discussed here will be constructed using a single deposition of evaporated aluminum. The thickness of aluminum of the DCRMS should be equal to the thickness of aluminum of adjoining SAW devices. Therefore, variations in thickness of the SAW devices should be detected by measuring the corresponding variations in the thickness of the DCRMS.

Generally line width variation of SAW devices is caused by the lithographic techniques used in constructing the device. The DCRMS will undergo the same photoresist exposure and other lithographic steps as the SAW devices on the wafer. Therefore, variation in the line width of the DCRMS should be proportional to variation in the widths of the fingers of the IDTs of the SAW devices. By measuring variation of the width and thickness of the components of the DCRMS, the variation of the mass of the fingers of the IDT may be determined.

By calibrating the relationship between the width and thickness (and therefore mass) of the fingers measured using optical and mechanical techniques and by measuring the centre frequency of the packaged SAW devices, the effect of variations in the mass of fingers of the IDT can be determined. Knowing this relationship, the variation in centre frequency of the SAW devices can be determined by measuring the dc electrical properties of the DCRMS.

The following is a discussion of the individual components of the DCRMS: the

SRS and the four LWS.

3.5.1 Sheet Resistance Structure (SRS)

The van der Pauw component (SRS) of the DCRMS is a simple 4-point electrical structure for determining sheet resistance. An example of the van der Pauw structure is given in Figure 11a. A current is applied to a square of conductive material at two points, and the resulting voltage is measured at the other two points. If a current, I_{13}, is applied to pads 1 and 3, the resulting voltage, V_{24}, is measurement on pads 2 and 4. A current applied to pads 1 and 2, I_{12}, would result in a voltage, V_{34}, being measured on pads 3 and 4.

Figure 11a (van der Pauw Structure - SRS)

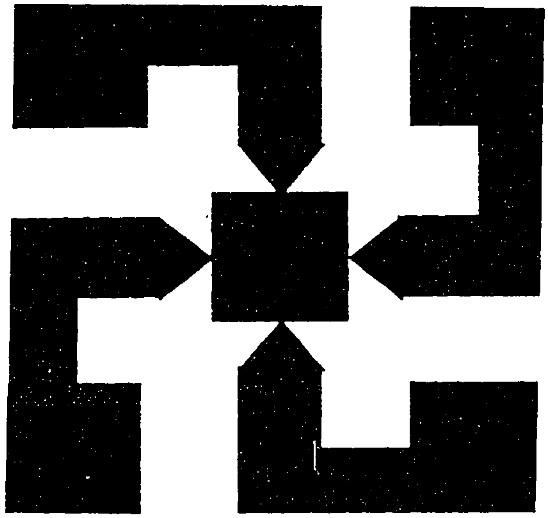

The resistance of the centre square for current I_{13} is equal to $R_1 = V_{24}/I_{13}$ and for current I_{12} is equal to $R_2 = V_{34}/I_{12}$. The sheet resistance (R_s) is calculated from

$$\exp\left(\frac{-\pi t R_1}{\rho}\right) + \exp\left(\frac{-\pi t R_2}{\rho}\right) = 1 \qquad (20)$$

equation 10.[28]

Using modern lithographic techniques, the centre square can be almost perfectly symmetrical. Therefore $R_1 = R_2 = R$.

Therefore

$$R_S = \rho/t = \pi/\ln 2 * R \qquad (21)$$

[28] L. J. van der Pauw, *Phillips Tech. Rev.*, 20 (1958), p. 220.

$\pi/\ln 2$ is a constant, so sheet resistance is proportional to the resistance measured using a current applied at two points and voltage measured at the opposite two points. Sheet resistance is defined as resistivity divided by thickness. Within a reasonable approximation, the resistivity of aluminum evaporated under the same conditions in the same evaporator should remain constant. So sheet resistance should be only dependent on the thickness of the aluminum deposition. Therefore, the thickness of the aluminum deposition is inversely proportional to the resistance measured on the SRS of the DCRMS.

3.5.2 Line Width Structure (LWS)

An example of the line width bridge structure is given in Figure 11b. A current, I, is applied to pads 2 and 4 of the line width structure.

Figure 11b (Bridge Structure – LWS)

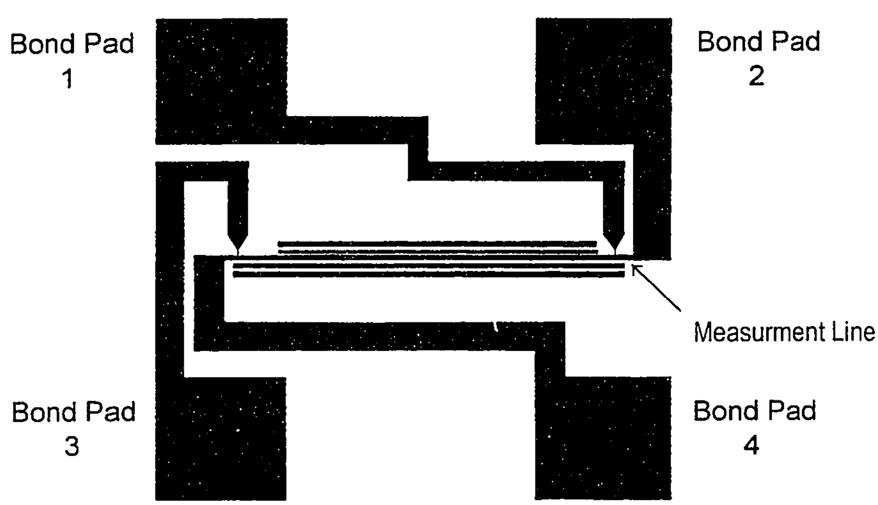

The voltage drop across the central line (measurement line) of the LWS is measured a distance L_{line} apart by measuring the voltage, V, on pads 1 and 3. The length, L_{line} , is the distance between the contact point of pads 1 and 3 to the central measurement metal line of the LWS. The length of this constant. Therefore the width of the line is determined by

$$W = R_S * L_{line} / R \qquad (22)$$

where R = V/I, where I is equal to the current I_{24} used to measure the resistance of LWS and R_S is the sheet resistance of the SRS. The variation of sheet resistance between the SRS and LWS of the DCRMS is negligibly small with modern processing techniques. Therefore, knowing the sheet resistance, R_s, of the SRS, the variations in the width of the line are known by measuring the voltage on pads 1 and 3 with an applied current on pads 2 and 4.

With four line LWS per DCRMS, line width variations for SAW devices with IDT finger widths ranging from under 1μm to over 10μm can be determined.

There are five lines inside each LWS. Of the five lines, only the resistance of the centre line is measured. The other four lines simulate the repeated pattern of a SAW device for the purposes of metal liftoff.

4.0 Equipment

4.1 Equipment Description

The DCRMSs and surface acoustic wave devices were fabricated by the Nortel Surface Acoustic Wave Device Fabrication facility. The DCRMS and the SAW devices were fabricated by depositing Al (with a 30 A Ti adhesion layer) on 42 degree centre seeded quartz wafers.

The dc measurement set up is shown in Figure 12. The dc structures were probed using a four point dc probe card. The coordinate layout for the contact points of the probe tips of the probe card is shown in Figure 13. There is a fifth probe tip shown in Figure 15 is actually a pair of probe tips used to determine if the probe card is making contact with the surface of the wafer. One of these probe tips is immediately above the other. When the bottom probe tip touches the wafer, it bends upwards to touch the top probe tip. This allows current to flow, thus informing the automated probing system that it is making contact with the surface of the wafer. It is not used for measuring the DCRMS.

The probe card itself is shown in Figure 14. The resistance of the dc structures was measured using a Hewlett Packard 34420A Nano Volt / Micro Ohm Meter. The dc structures were probed on 3 inch quartz wafers mounted on a Rucker and Kolls 680A Series Semi-Automatic Wafer Prober.

Figure 12 (Manual DC Measurement Setup)

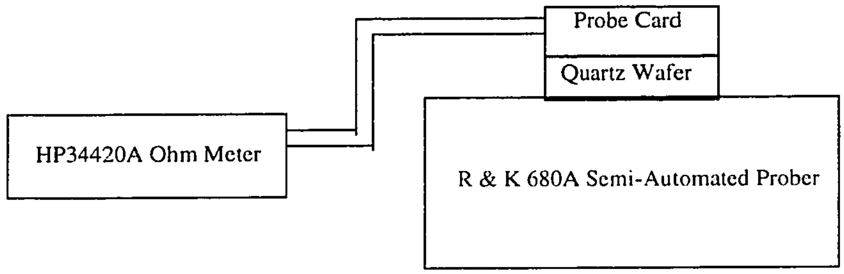

Figure 13 (Coordinate Layout of the Probe Tips of the DCRMS Probe Card)

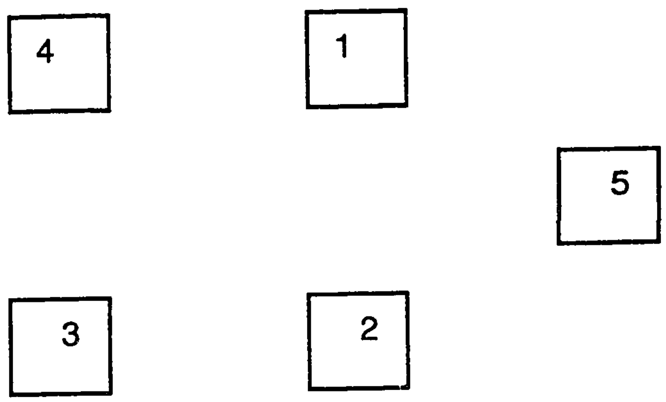

Pt	Coordinate in inches	Function
1	(0.0236), (0.0236)	+ signal lead on right side
2	(0.0236), (0.0000)	- signal lead on right side
3	(0.0000), (0.0000)	- signal lead on left side
4	(0.0000), (0.0236)	+ signal lead on left side
5	(0.0354), (0.0118)	EG Edge Sensor

Figure 14 (DCRMS Probe Card)

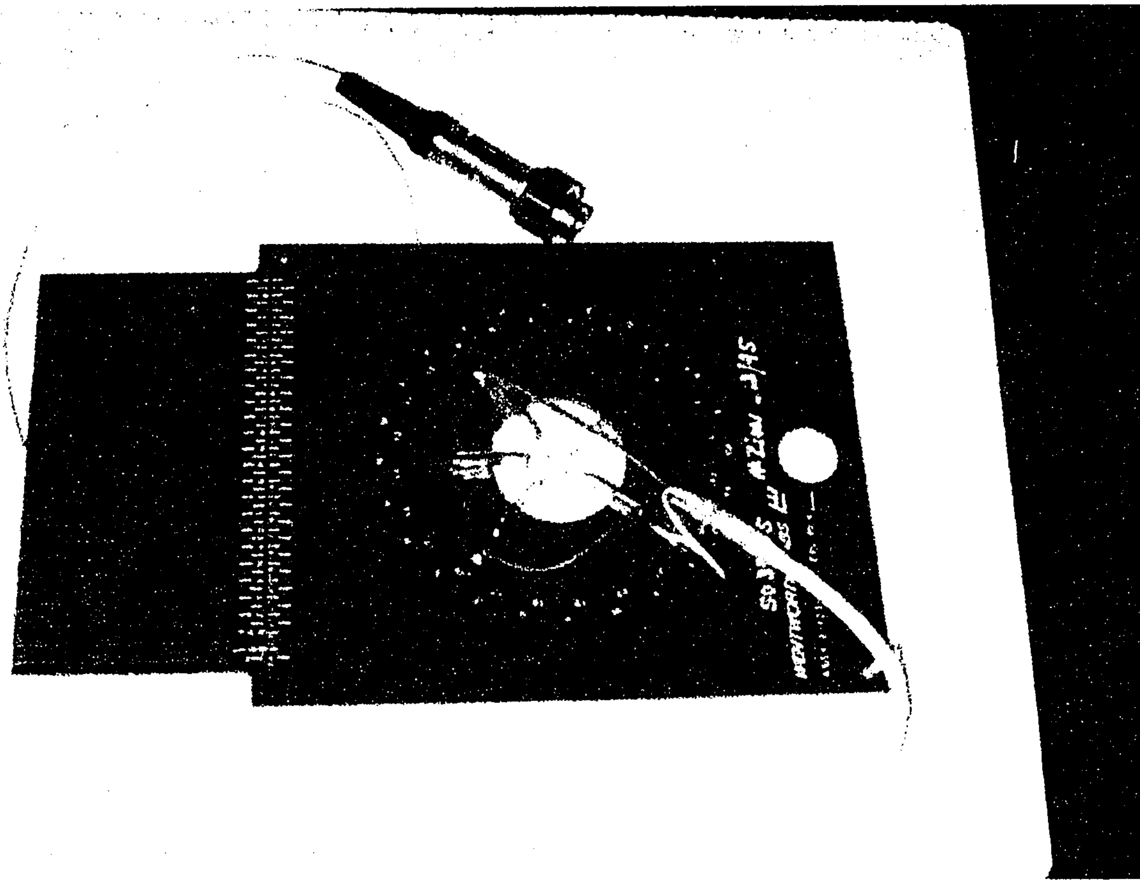

The SAW devices were measured by the automated probing set up shown in Figure 15. A picture of the setup used for the RF die probing of the SAW devices is shown in Figure 16. The RF measurements were made directly on the SAW devices using ground plane single RF probes (44-MANP-S-GP (right) and SPP9309008 (left)) manufactured by Micromanipulater Inc. (Figure 17). The RF properties of the SAW devices were measured using a Hewlett Packard 8752A Network Analyzer. The processed quartz wafers containing the SAW devices were mounted on a Rucker and Kolls 680A Series Semi-Automatic Wafer Prober. A Pentium PC was used to automate the RF measurements of the HP Network Analyzer and the movements of the R & K Wafer Prober.

Figure 15 (Automated RF Measurement Setup)

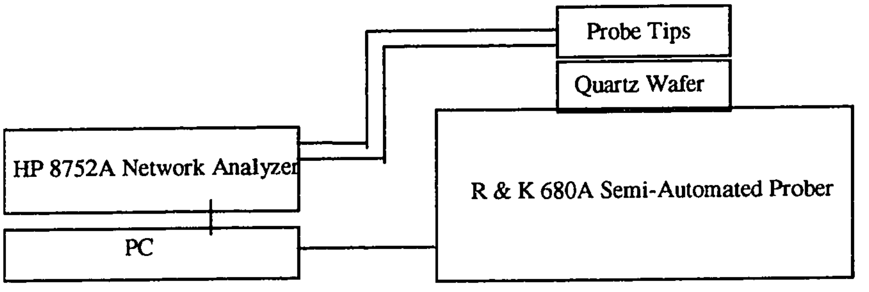

Figure 16 (RF Probing Setup)

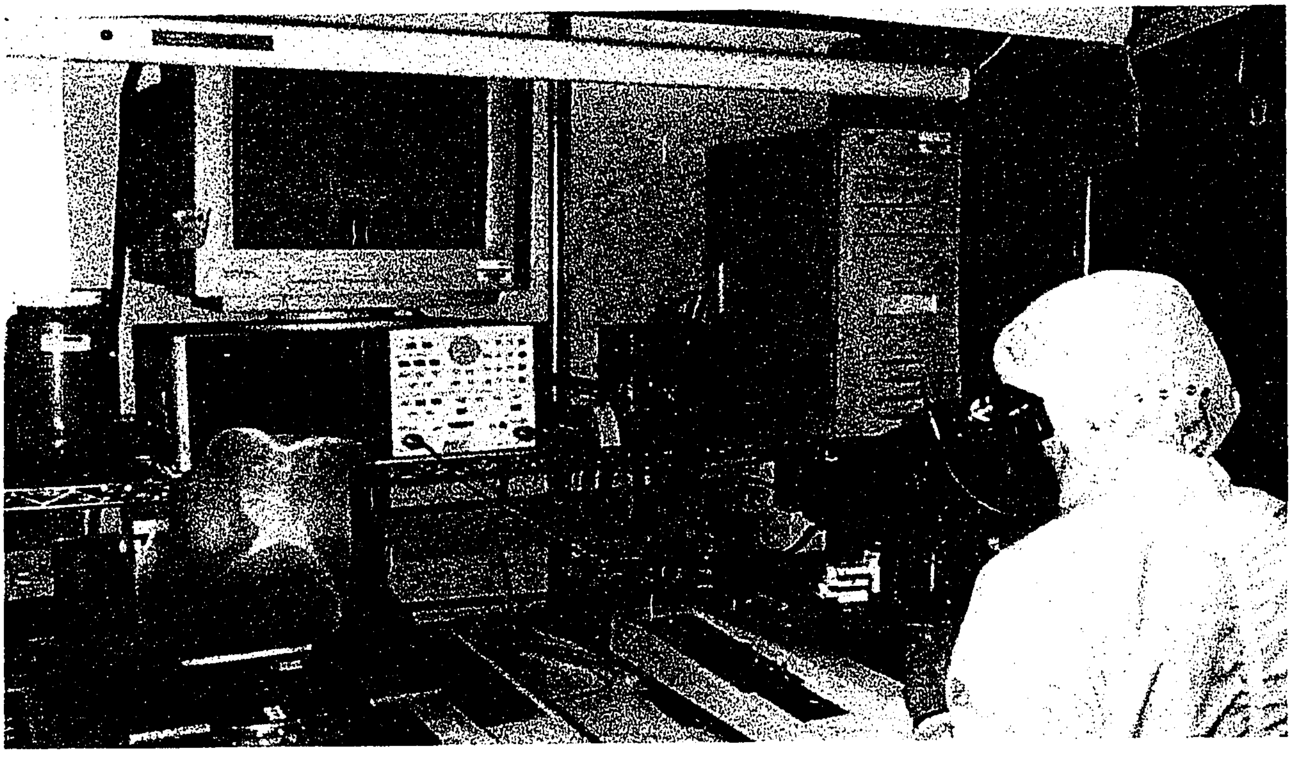

Figure 17 (Micromanipulators Left - 44-MANP-S-GP Right - SPP9309008)

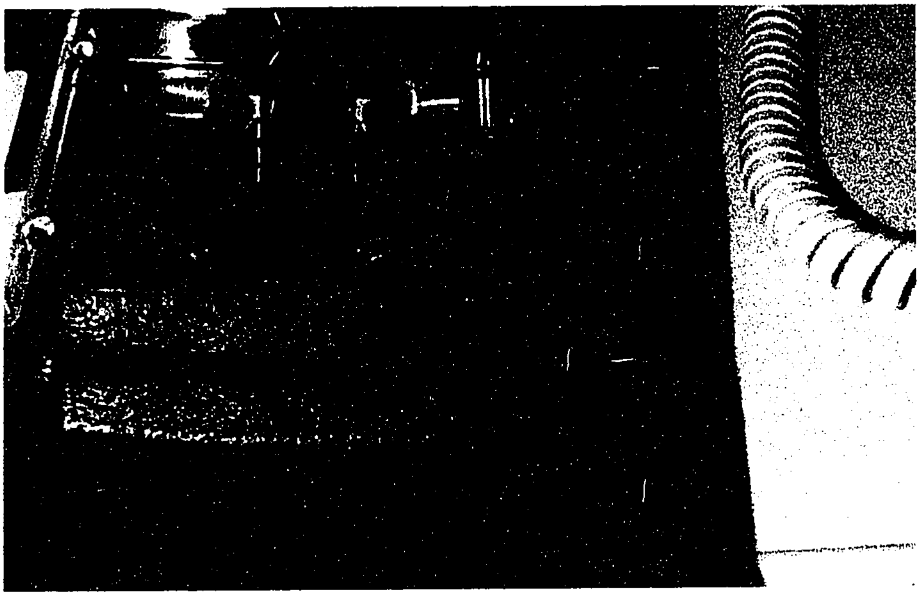

A close up of the actual probing of a SAW device can be seen in Figure 18. In this picture, one can see the placement of the probe tips on the surface of a wafer of SAW devices.

Figure 18 (Close Up of Automated Die Probing of SAW Device – with Inker)

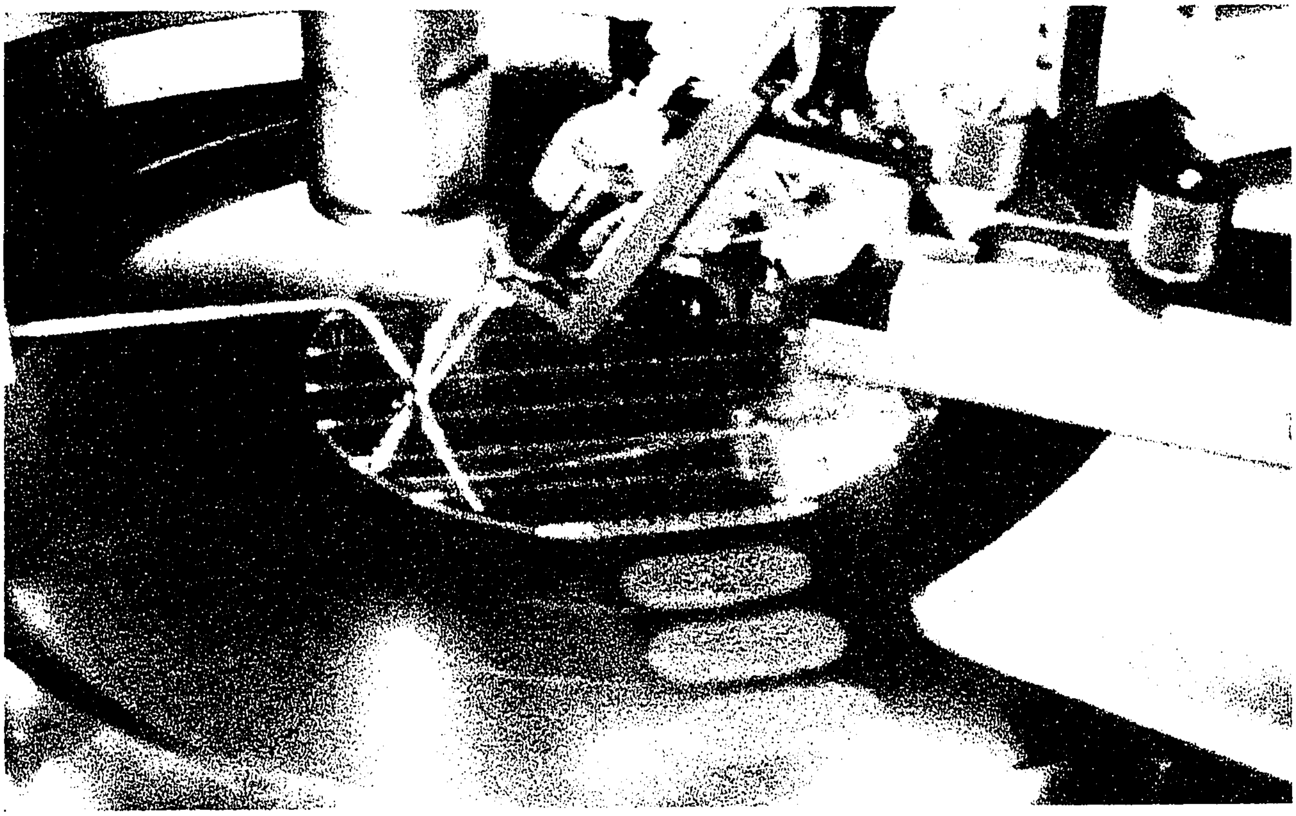

The line widths of the LWSs were measured optically with the OSI Microvision 500 Measurement System. The OSI system measures the width of lines by measuring the changes in light intensity reflected from the sample. The metal thicknesses were measured using the Tencor P-10 Surface Profiler. The P-10 surface profiler physically measures the metal thickness by scanning a metal stylus p over the sample.

4.2 Automated RF Die Probing of SAW Devices

4.2.1 Mechanics of RF SAW Die Probing

The RF probing set described in Figure 13 and shown in Figure 14 was developed for the sole purpose of RF probing a SAW device in a computer automated fashion.

The SAW devices on a wafer are laid out in a regularly spaced pattern. Each section of the pattern containing the smallest repeated feature, usually one SAW device, is called a die. To be packaged, a die is cut from the wafer and mounted into a package. What is known as die size, is the vertical and horizontal dimensions of the die. Each die has another die touching each of its sides. This forms a grid pattern of dies with unit sizes equal to the die size.

The repeated pattern is extremely useful for RF probing of the die. Since each die is a consistent and exact distance from its neighbors, a system can probe each die by moving the probes in the pattern of the particular wafer. In short, an operator can set up the probe tips on the first die and the computer will instruct the prober (R & K 680A in this case) to move from one die to the next.

For each die, the computer will instruct the prober to lower the tips onto the die. Then the computer will instruct the network analyzer to take a measurement. The results from the network analyzer's measurement will be returned to, and stored in, the computer. Finally the computer instructs the prober to raise the probe tips and to move to the next die in the pattern.

This system allows for the automated die probing of an entire wafer of SAW devices with no chance of mechanical error (dropping the probe tips on a location other than the electrical bond pads). The system shown in Figures 13, 14, and 15 was constructed for the purpose of automated probing of SAW devices.

The probing of a wafer of SAW devices is fairly simple, because the pattern is repeating. However, the SAW devices are eventually cut or diced into individual die. Because SAWs are propagated on crystals, SAW devices are very susceptible to variations in stress and boundary conditions (reflections from at the boundary of the surface of the die) of the crystal.

To most accurately determine the exact RF characteristics of the SAW device, the die would need to be probed in cut die form. Since the die is no longer in wafer form, the regular pattern has been lost. Historically, the die would be individually probed by hand by a bank of test technicians. This method is very slow and labour intensive.

Another feature was developed for the system shown in Figure 14, to deal with this problem. Before a wafer is cut, it is placed on stretched blue adhesive tape. This tape is holds the die together while the wafer is being cut with a water saw. Once completed, the die are no longer touching one another. The tension on the tape causes it to stretch, pulling the die away from one another.

It can assumed that the tape stretches fairly uniformly, especially over a small region. An algorithm was developed to take this tape stretching into account. Once the test technician has set up the probe tips on the first die, the computer walks the probe tips through a simple pattern. From the original pattern of the die on the wafer, the computer chooses six other die on the same wafer. The first die itself is always chosen to be the far left die in the bottom row of the wafer. The computer then determines which die is the furthest to the right on the same row. The next three dies chosen by the computer are the far left, far right, and centre die of the middle row of the pattern of SAW devices. The last two dies chosen are the far left and far right dies on the top row of the pattern of SAW devices.

The computer instructs the prober to move to each one of the dies. At each die, the probe tips no longer line up properly over the bond pads. The test technician uses the prober to move over to the correct position. The computer records the coordinates of the movement needed to move the tips over the bond pads. The procedure is repeated for the six chosen dies. From the recorded shifts, the program does a linear interpolation of the shifts in between these points. This assumes that the stretch is fairly uniform and that the die properly adheres to the tape.

When the computer begins probing the cut die, it uses the linear interpolation of the shifts to determine the location of each die. Using these interpolated locations, the prober is able to probe all of the cut dies. This is the action taking place in Figure 16.

Over an entire three inch wafer, the probe tips are accurate to about 10 μm of the bond pad centre. This is more than enough when the bond pads are normally over 100 μm wide. The theory and the system were developed by the author in parallel with the work in this thesis. To date, this system (and its clones at Nortel), are the only ones of their kind in the world.

This method would seem to have its advantages over the DCRMS for measuring the properties of SAW devices. However, this system requires a specialized probing arrangement for each different SAW device design. While the DCRMS can be applied to different SAW devices using the same pad arrangement. Furthermore, many SAW devices require matching components to probe properly. The DCRMS is a dc measurement and does not need matching components. The SAW device tested in later sections by the test system happens to have a pad layout and match conducive to automated RF probing.

4.2.2 Electrical Specifics of RF Probing of SAW Devices

All of the RF measurements discussed in this paper were made using the probe tips shown in Figure 15 (or with probe tips identical to those). The centre frequency, bandwidth, and insertion loss measurements were obtained from S21 transmission measurements. S21 is the ratio of the intensity of the signal transmitted through the die over the intensity of the signal input into the die.

The insertion loss is the maximum S21 value of the measurement. This is the S21 amplitude at the frequency of maximum transmission. To measure the bandwidth, the network analyzer measures the two frequencies where the transmission (S21) amplitude of the signal is a defined amplitude (or attenuation) from the maximum of the transmitted signal. The defined amplitude is known as the marker width. The marker width is the attenuation relative to the minimum insertion attenuation of the signal (see Figure 19), at which the bandwidth is measured. For a marker width of –5 dB (chosen by the individual conducting the measurement) and a device with an insertion loss of –7 dB, the two frequencies chosen would be the frequency of the bandpass shape with an amplitude of –12 dB. The marker width is chosen to match the particular desired pass band attenuation. It is a semi-arbitrary value dependant on the desired performance (pass band) of the SAW device.

The bandwidth is the difference between those two frequencies measured at the desired attenuation. The centre frequency is the average of the two frequencies. Figure19 provides a visual description of most of the SAW band pass filter terminology.

Figure 19 (SAW Band Pass Filter Terminology)[29]

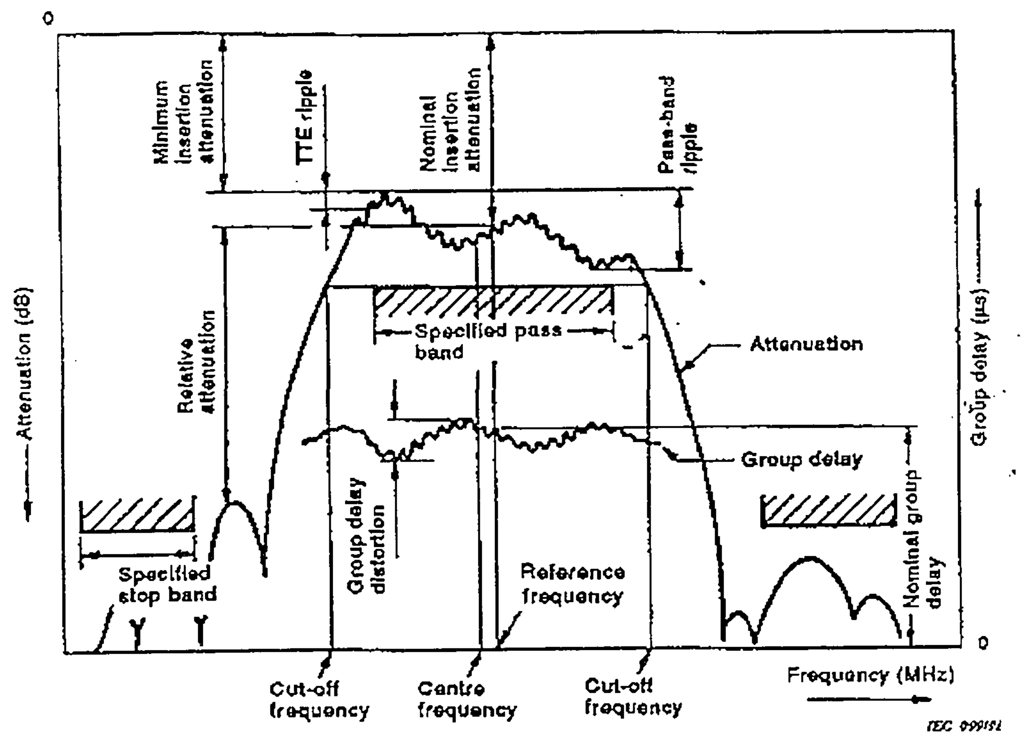

As an example, a device is measured with a marker width of –5 dB. The device being measured has an insertion loss of –7 dB. For the device, the two frequencies measured at –12 dB are 838.1 MHz and 840.3 MHz. The bandwidth of the device at –5 dB (marker width) is 2.2 MHz and the centre frequency of the device at –5 dB is 839.2 MHz.

For the SAW devices measured in this paper, there are a number of reflections that need to be filtered to obtain the true centre frequency and bandwidth of the device.

---

[29] **Surface acoustic wave filters. International Standard. Bureau Central de la Commision**

The reflections are mostly caused by matching problems to do with the unpackaged die. The die chosen for this paper is relatively simple and can have its reflections filtered by the network analyzer.

The reflections generally arrive at the detector in the network analyzer at different times. By only accepting signals arriving in a set window of time, the reflections can be filtered. This is called time gating. A lower and upper limit in time is set (start and stop time gates). Only signals that arrive in this interval will be included in the measurement. The network analyzer fourier transforms the time domain information obtained between the start and stop time gates into the S21 frequency measurement.

The SAW device chosen in this paper has a chosen marker width of –5 dB. The start and stop time gates used for the measurement of this SAW device are 0.5 μs and 1.5 μs respectively.

Electrotechnique Internationale, CEI IEC 862-1. 1989, p. 21.

5.0 Process Information

The dc measurement structures were developed to monitor process variations in the fabrication of SAW devices. Specifically, the DCRMS structure was created to monitor the variation in the metal thickness and the line width of SAW devices between wafers.

5.1 Aluminum Deposition

The variation of metal thickness is caused by variations in the Al deposition. Each SAW device design has a target Al metal thickness for the desired target centre frequency. Wafers containing the same particular device design have Al deposited at the same target thickness.

The aluminum evaporator controls the thickness of the Al deposited using a quartz crystal sensor. The quartz crystal sensor changes frequency with changes in deposited Al thickness.

Wafers with Al deposited at the same time (same batch) generally have the same metal thickness. However, there is variation in metal thickness between different batches (different evaporator runs). The SRS component of the DCRMS was designed to measure the variation in metal thickness between wafers in the same batch (theoretically very small) and between wafers from different batches.

The optimum use for the SRS is for it to determine the variation in metal thickness within a wafer. This will hopefully help determine the spread of frequencies in a wafer (from the variation in metal thickness across the wafer).

5.2 Line Width Variation

The term line width denotes the width of the line of the IDT.

The line width variation is dependent on the photolithography line widths. During the fabrication of the SAW devices, the line width of the metal lines is principally dependent on the exposed photo resist pattern. Photo resist is deposited on a wafer. A pattern is exposed on the wafer using UV light (Figure 20a). The photo resist is developed and the photo resist dissolves in the locations where it was exposed (Figure 20b). The metal lines, later in the fabrication process, form in the locations where the photo resist has been removed (Figure 20c).

Figure 20a

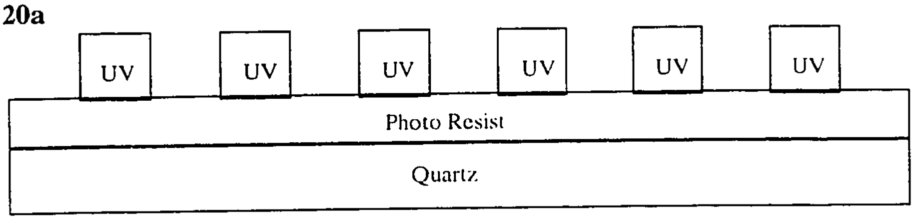

Figure 20b

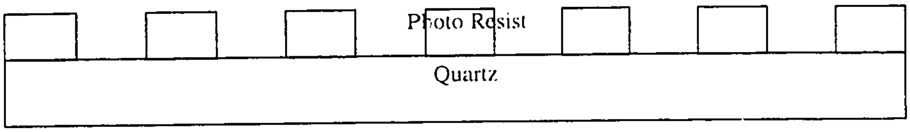

Figure 20c

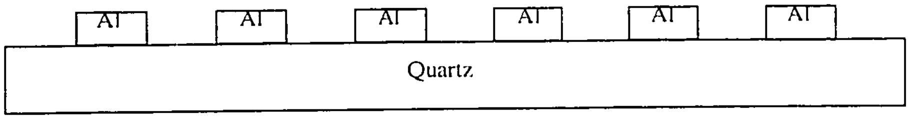

By changing the width of the lines in the photo resist that are exposed, the width of the final Al lines can be varied.

The line widths of the SAW devices and of the LWSs were varied by varying the exposure energy of the UV light incident on the photoresist. The exposure energy is the total energy of the UV light incident on the photoresist.

A pattern is formed be placing a mask over the photo resist covered wafer. The UV light is projected through the mask onto the photo resist. The photo resist directly in the path of UV light is exposed. The photo resist at the edge of the UV path (Figure 21) is exposed slowly by indirect UV light. This 'bleed' through effect is slower than the direct path exposure. By varying the total energy of the photo resist exposure, more or less of the photo resist outside of the direct path of the UV light will be exposed. Since the line width of the final Al lines is dependent on the exposed photo resist line widths, increasing exposure energy leads to wider lines.

Figure 21 (Effects of Indirect Exposure)

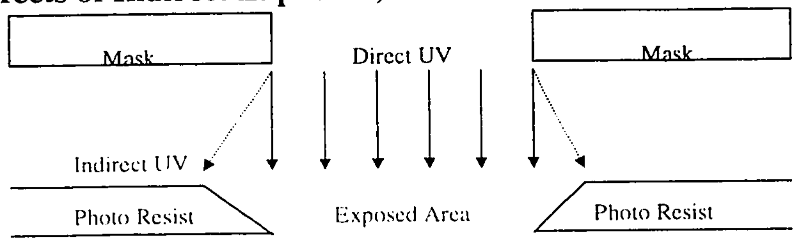

The increasing and decreasing of exposure energy is an effective method of artificially changing the width the of the line of the IDTs. In practice the variation in line widths originate from sources other than exposure energy. A major cause of line width variation is changes in the thickness of the photoresist.

If the thickness of the photo resist changes, the line width changes. For thinner photoresist, the area cleared by indirect light will increase (the indirect light does not have to expose as deeply into the material – less energy needed to clear to the surface). For thicker photoresist, the area cleared by indirect light will decrease (the indirect light has to expose more deeply – more energy needed to clear to the surface).

As a controlled means of line width variation, variation of exposure energy was chosen over variation of photoresist thickness. Variations in exposure energy are easier to re-produce and more consistent across the wafer than variations in photoresist thickness.

6.0 Experiment

6.1 Fabrication

Four different DCRMS fabrication runs were conducted. A run is a batch of wafers fabricated at the same time. There were two to four wafers per fabrication run. The DCRMSs were fabricated on 3 inch diameter, 42 degree seeded quartz wafers. Two of the fabrication runs of DCRMSs were conducted with a target Al metal thickness of 450 A. One fabrication run of DCRMSs was conducted with a target Al metal thickness of 500 A. The fourth run of DCRMSs was conducted with a target Al metal thickness of 1000 A.

Each wafer in a DCRMS fabrication run was covered with an evenly-spaced, repeating pattern of DCRMSs. Each fabrication run had the metal deposited in the same chamber at the same time. This leads to wafers in a run having similar metal thickness.

6.2 Comparison of Measurement Tools to Scanning Electron Microscope

One of the most accurate methods of measuring the width and thickness of the line width structures is by using a scanning electron microscope (SEM). However, the cost of SEM measurements is about $400 / hr. Measuring the metal thickness at one site and the four line widths at five sites on a wafer takes 3 to 4 hr. For cost reasons, this is impractical.

A cheaper method of measuring the line width of rectangular metal lines is the use of an optical measurement tool, such as the Microvision measurement tool described in Section 4. By measuring the changes in reflected light intensity of a highly reflective surface (aluminum on quartz), the optical measurement tool can determine the width of one reflective material on another (aluminum on quartz). One drawback to this tool is that as the width of the structure being measured approaches the wavelength of the incident light, the quality of the measurement degrades due to diffraction effects.

A cheaper method (than SEM) of measuring the metal thickness of the aluminum structures on quartz is the use of a mechanical profiling tool such as the surface profiling tool mentioned in Section 4. This tool scans a stylus along the surface of a structure. The tool monitors changes in the height of the tip throughout the linear scan. By averaging the needle height at the top of an aluminum structure and by averaging the needle height at the quartz surface, the height of the aluminum structure can be determined. One drawback to this method is that the line height measurement is for only one cross-section of the structure, not the average metal height of the structure.

An advantage of both tools compared to the scanning electron microscope, is that they are non-destructive. Measurements using the scanning electron microscope require coating the sample with a thin layer of conducting material. After being measured with the optical and profiling tools, the sample can continue in production. Following measurement with the SEM, the sample is no longer usable. Using the optical and profiling tools, the width and thickness of the Al structures can be measured and the same structure can subsequently be measured electrically and/or packaged.

Section 6.2.1 and 6.2.2 are concerned with evaluating the effectiveness of the optical and profiling tools relative to the 'standard' of the scanning electron microscope. The optical and profiling tools need to be calibrated against the SEM to determine if these tools are adequate for use as a standard against the line thickness and line width measurements obtained by of the DCRMS.

Optical line width and mechanical metal thickness measurements were conducted for three wafers. The metal thickness for an SRS on each wafer was measured using a SEM. The linewidth of the four LWSs on two DCRMSs (one at the edge, one at the centre) for each wafer were measured using a SEM. The same structures had metal thicknesses measured mechanically and line widths measured optically.

6.2.1 Comparison of Profiling Tool Thickness Measurements to Scanning Electron Microscope Measurements

To measure the thickness of the metal line, the wafer was cleaved through the square pad in the centre of a SRS. A sample SEM photo is shown in Figure 22. The thickness was measured by drawing a line along the top surface of the SRS centre pad on the SEM display (upper horizontal line of Figure 22) and drawing a line along the surface of the quartz wafer (lower horizontal line of Figure 22). The measured thickness is the distance between these two parallel lines.

Figure 22 (SEM of Cross-section of the Centre Square of a SRS)

(The sloping bright white shape is the edge of the aluminum pad)

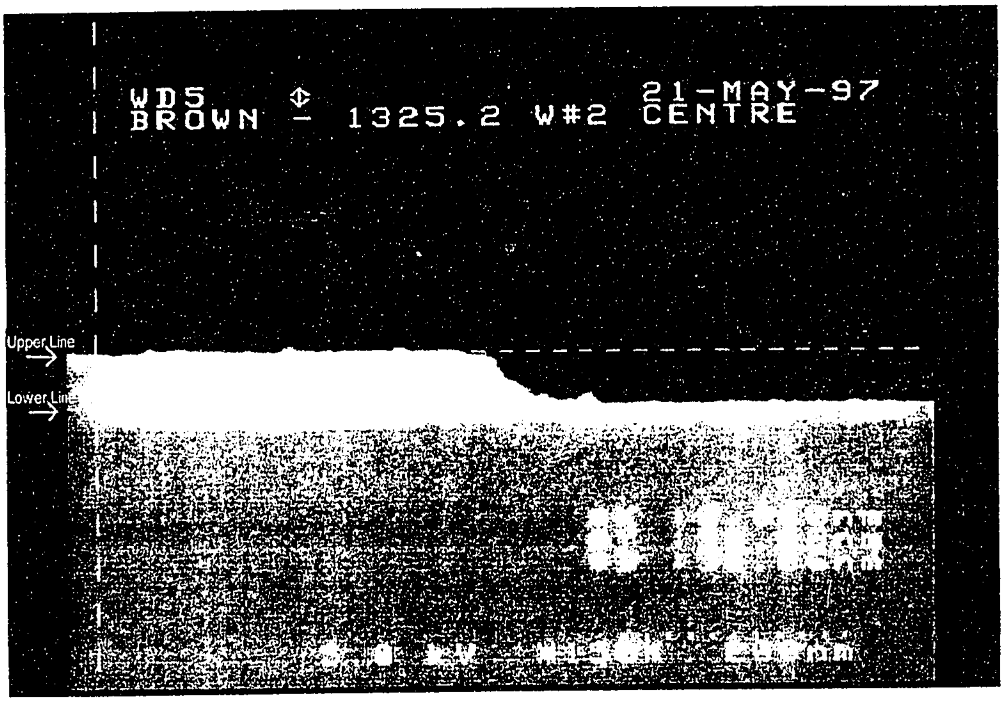

Notice that the edge of the metal pad is not perpendicular with the substrate surface (ie. the curved slope in the middle of Figure 22). This slope is an effect of the fabrication process. The sloped edge is proportionally very small compared to the size of the pad and is averaged out when making line width measurements (see the next section).

The mechanically measured (surface profiler) metal thickness and the SEM measured metal thickness are shown in Table 1.

Table 1 Comparison of SEM and Surface Profiler Thickness Measurements

SEM Measurement (+- 5 A)	*Surface Profiler Meas. (+- 10 A)*	*Difference (+- 15 A)*
480 A	514 A	34 A
467 A	514 A	47 A
510 A	549 A	38 A

There seems to be a consistent thickness difference between the SEM thickness measurement and the surface profile measurement. The mechanically profile measurement is roughly 40 A larger than the SEM thickness measurement for thicknesses near 500 A. This shows a discrepancy between the mechanical measurement and the SEM.

If Figure 22 is closely scrutinized, some deviation between the substrate surface and the parallel line used to measure thickness is seen. The difference between the parallel line and the surface is small, but could be enough to cause a small offset. The SEM measurements were conducted consistently, so the relative variation should be the same as the relative variation for the mechanical thickness measurement.

Even though the SEM and the mechanical profiler have measured different metal thicknesses, the difference between the two seems consistent. Despite the fact that the absolute measured thickness may differ from that of the SEM, the mechanical profiling tool is an effective tool for measuring the variation in thickness of a metal line.

The mechanical profiling tool is accurate enough to be used as a comparison to the SRS. The mechanical profiling tool will be used for all metal thickness measurements for the rest of this document.

6.2.2 Comparison of Optical Line Width Measurements to Scanning Electron Microscope Measurements

The line width for four LWSs from two different DCRMSs (one at the centre, one at the edge) was measured using a SEM, viewing the line from above. To be more specific, the 1, 2, 5, and 10 μm LWSs for a DCRMS at the centre of the wafer and for a DCRMS at the edge of each wafer were measured. This is to take into account any variation of metal thickness or line width between the centre and the edge of the wafer.

The greatest discrepancy between SEM and optically measured line width was expected for the 1 μμ line. The OSI optical measurement tool becomes less accurate as the line spacing approaches the wavelength of visible light (~ 0.5 μm). The accuracy of the optical measurement tool should be least accurate for the 1 μm LWS (compared to the three LWS sizes). Figure 23(a – d) contains four SEM photographs; one for each line width measurement.

Figure 23a (SEM Photograph of 1 μm LWS)

(The two crosses are displayed on each side of the 1 μm metal line. The measured line width is the distance between the two crosses.)

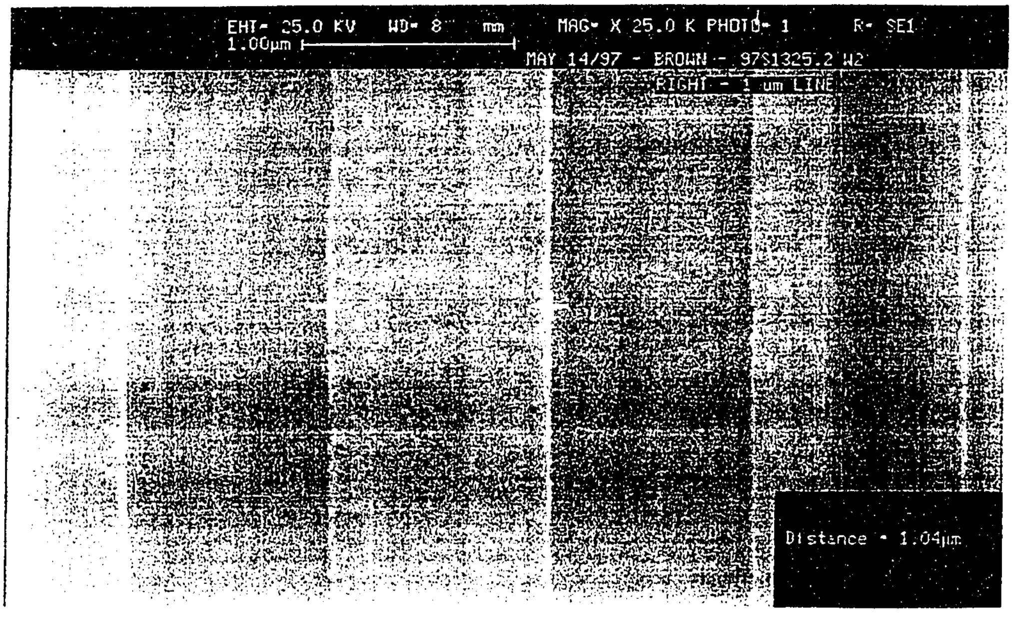

Figure 23b (SEM Photograph of 2 μm LWS)

(The two crosses are displayed on each side of the 2 μm metal line.)

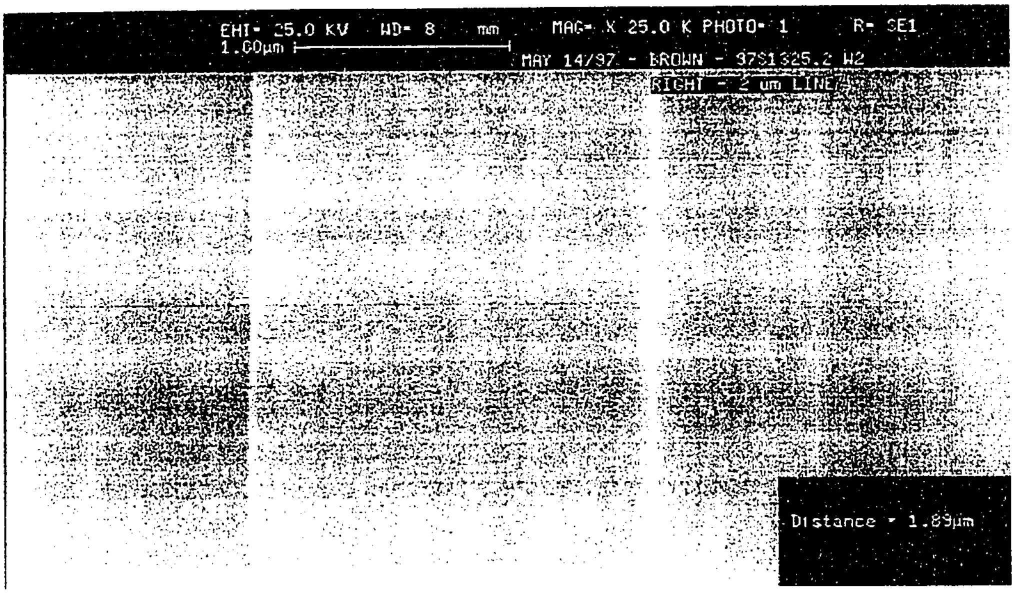

Figure 23c (SEM Photograph of 5 µm LWS)

(The two crosses are displayed on each side of the 5 µm metal line.)

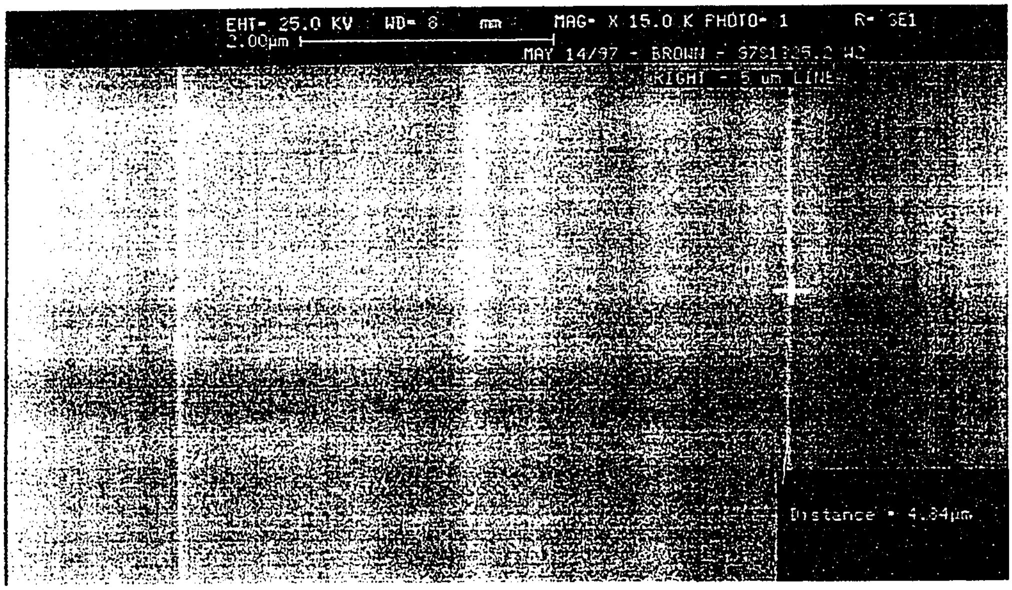

Figure 23d (SEM Photograph of 10 μm LWS)

(The two crosses are displayed on each side of the 10 μm metal line.)

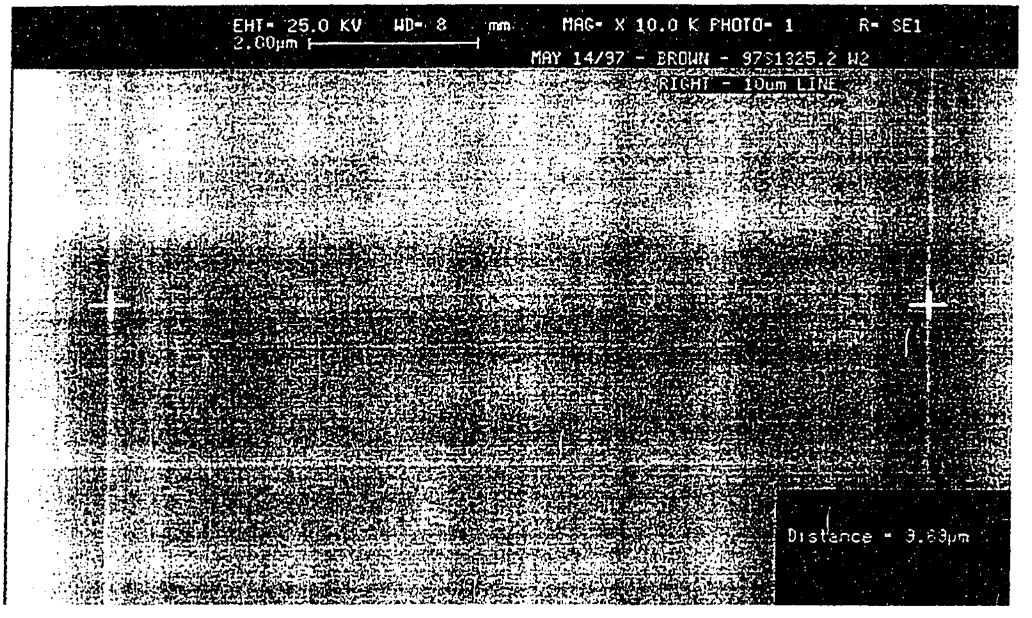

The line widths were measured, using the SEM, by placing a marker (two crosses shown in Figures 23a to 23d) at the edge of the haze of the displayed line. This haze (white lines marking the edge of the metal lines) is partly due to the sloping edge of the line caused by the fabrication process and partly due to the diffraction at the edge of the structure.

The convention of measuring the line width using the optical tool is to calculate the width from the inflection point of the sloping edges (Figure 24). This results in a smaller measured line width than by SEM methods. However, this method of optically measuring line widths is more representative of the effective line width of the structure.

Assuming a linear slope, taking the line width measurement from the midpoint of the sloping edges(at height x, where x is ½ the height of the line) yields a rectangle with the same area as the trapezoidal cross-section of equal height and midpoint width.

Figure 24 (Measurement of a Metal Line)

(Sketch of a the cross-section of a lithographically patterned, evaporated aluminum line)

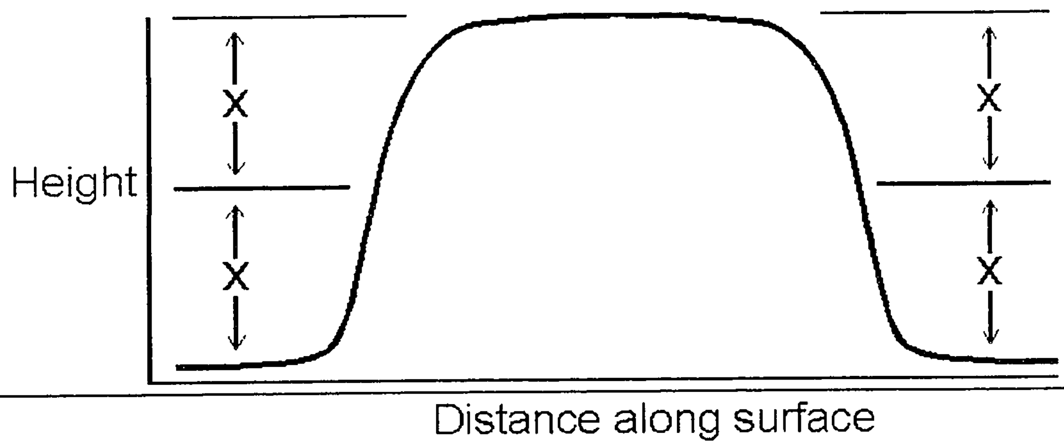

Figure 25 shows a graph of the optical measurement to the SEM measured line width for the 1 μm LWS. The purpose of this comparison is to determine the effectiveness of the optical measurement tool. The smaller the line width, the greater the chance of measurement error with the optical measurement tool (as the width of the line approaches the wavelength of the incident light), the SEM / Optical measurement values were compared for the LWS with the thinnest line width. This gives a conservative estimate of the potential difference in measured line width values.

Figure 25 (SEM Measurement for 1 µm LWS)

(The optically measured line width versus the SEM measured line width. Each point represents a different line. All of the measured lines were chosen from across the same wafer.).
Top Line: Theoretical line from 1:1 correlation of optical measurements and SEM measurements.
Bottom Line: Theoretical line from 1:1 correlation of optical measurements and SEM measurements with an offset of 30 nm between the measurements.

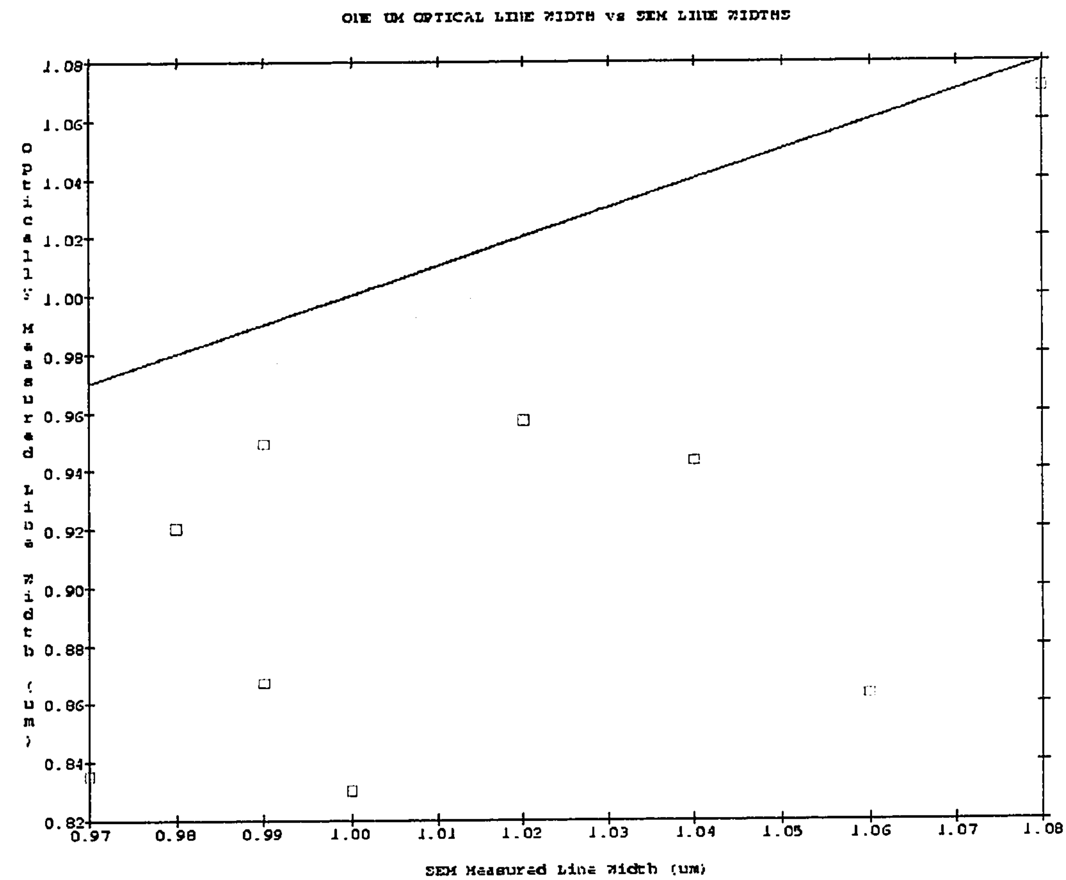

A solid line on Figure 25 represents a theoretical 1:1 ratio of optically measured to SEM measured line width. As expected, the average optically measured line width is less than the SEM measured line width (centre of sloping edges compared to the bottom of the sloping edges). From the SEM thickness photograph (Figure 22), the sloped edge can be determined to be roughly 30 nm in width. If the SEM line width measurements were made from the centre of the hazy edges (roughly half way along the sloped edges), the measured line widths would be roughly 15 nm smaller. A second line is drawn on Figure 25 approximating a 0.015 μm offset between the optical and SEM measurement.

This second line is closer to the optically measured data. However, the optically measured 1μm line widths are smaller than even the offset 1 μm SEM line width measurements. The optically measured line width is, on average, within 0.082 μm of the offset SEM 1 μm line width measurement. The standard deviation of this difference is 0.062 μm.

The desired accuracy is 10% of the line width. Assuming a Gaussian distribution, 95% of the points should be within two standard deviations (or +-0.124 μm) of the centre. This is roughly 12% of the line width. The optical method, is barely good enough for the task (the SEM measurements are as close to perfect as reasonably possible).

One problem with both methods, is that both measure the line width at one section of the metal line. This assumes that the metal lines are of uniform thickness. In reality, the lines are a bit rough (the fabrication process is not perfect), so the SEM and optical measurements do not necessarily represent the line width, only the width of that particular section of the line. In general practice, it has been seen that the width of the line at one section is an effective approximation to the average width of the metal line, since the line should have a fairly uniform width.

6.3 Verification of DCRMS Relative to Ohm's Law

6.3.1 Verification of the Line Width Structures

The first step in determining the effectiveness of the DCRMS was to verify the basic theory (in terms of Ohm's Law). Theoretically, the dc resistance of components of the dc measurement structure is inversely proportional to the volume of Al (assuming constant resistivity and density). The Al is deposited under identical conditions in every run, therefore resistivity and density can be assumed to be constant. However, at a certain point a resistance minimum will be reached. The volume of Al can only become so large before the dc resistance stops being inversely proportional to Al volume, as the path of the electrical current will take the shortest distance between the two probes.

For example, if the same experiment took place with a 1 m by 1 m by 1 m metal structure and a 10 m by 10 m by 10 m metal structure. The 10 m by 10 m by 10 m structure would not have 1/1000 of the resistance of the 1 m by 1 m by 1 m structure. The relationship is only linear within a certain range (small resistance limit). However, for a 1 µm by 1 µm by 1 µm structure and a 2 µm by 1 µm by 1 µm structure, the second structure should have 1/2 the resistance of the first structure. The relationship deviates more from linearity as the metal becomes thicker. The shortest path for the electrical current would be from contact to contact, not through the depth of the material.

This is most relevant in terms of the 1, 2, 5, and 10 µm line width structures. The linearity of the relationship of the resistance of the LWS between all four LWSs (1, 2, 5, and 10 µm) had to be determined. The first data processed were used to determined that the linear relationship for the four line widths is true, at least up to a Al thickness of 1000 A.

The dc resistance of the centre structure (SRS) of each DCRMS was measured. The line width of each LWS was measured optically. For each line width structure, the dc line width resistance was measured. The SRS of the corresponding dc centre resistance structure was divided by the dc resistance of the particular line width structure (one of the four LWSs attached to the DCRMS) and plotted against the corresponding optically measured line of width of the same LWS (Figure 26).

Figure 26 (Linear Relationship of the DC Resistance of the Four LWSs)

(Each point represents a SRS site. The SRS sites were measured at multiple locations on multiple wafers. The curve fit is used as the four structure curve fit for Figures 26 to 29.)

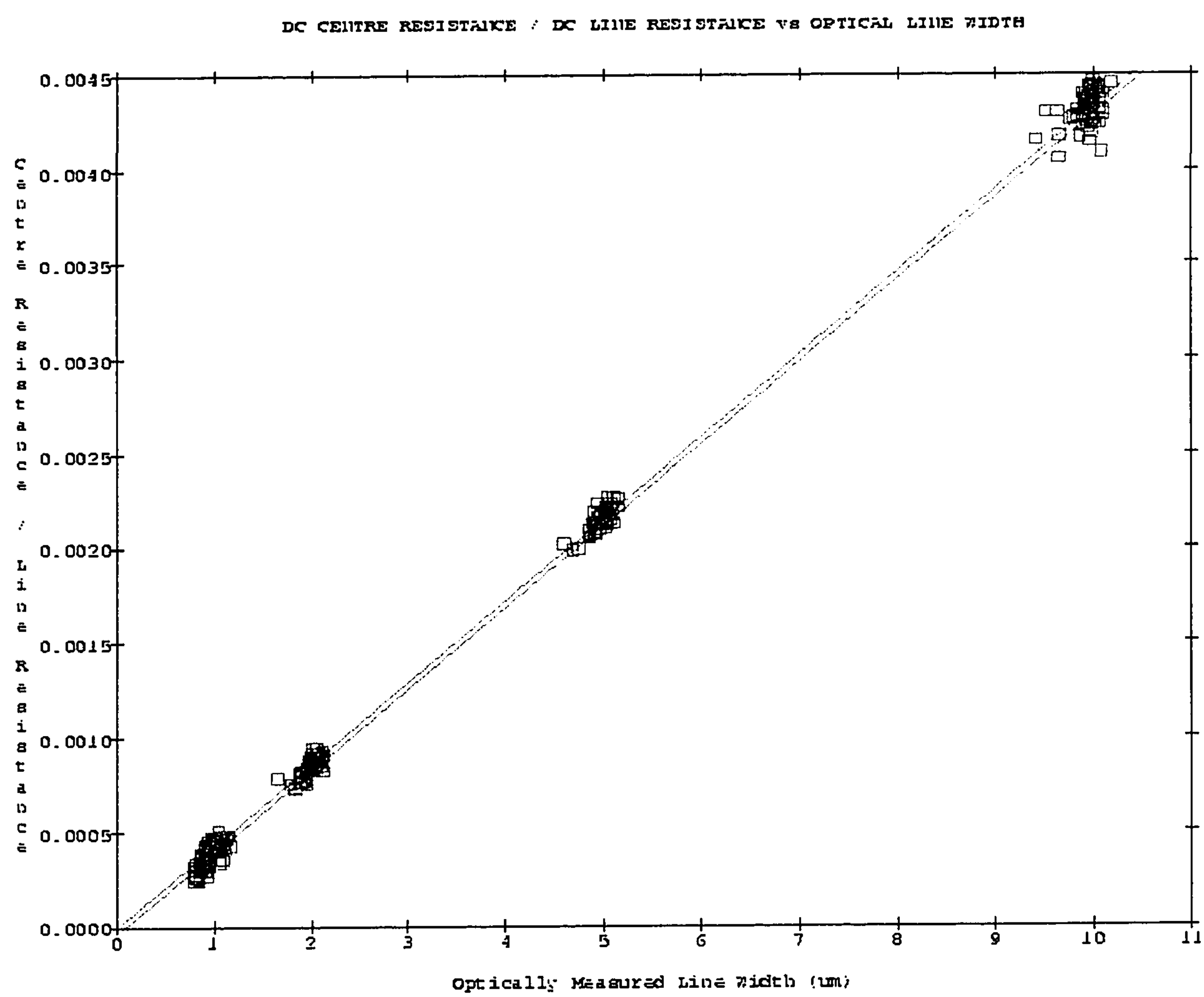

The dc centre resistance (resistance of SRS) / dc line resistance versus the optically measured line width fits well to a line when all four line width structures are graphed together. This proves that the application of Ohm's Law to the line width structures is correct and that the large volume limit (small resistance limit) has not been reached by the fabricated DCRMS (up to 1000 A metal thickness). The curve fit to Figure 26 gives a linear fit for the relation of dc centre resistance / dc line width resistance to optically measured line width of (4.328 +- 0.212) * 10^{-4} * (optically measured line width in A) – (3.1 +- 15.1) * 10^{-5}. The curve is not perfect as the y-intercept should be 0 microns (it is -3.1 * 10^{-5} microns), however a y-intercept of zero is within the uncertainty of the measurement. It fits well to the data for four fabrication runs (14 wafers). By inverting the curve fit, the line width should be [(2.310 +- 0.113) * 10^{3} (dc centre resistance / dc line width resistance) + 7.1 * 10^{-2}] microns.

Figures 27 to 30 show dc centre resistance / dc line width resistance against the optically measured line width for a particular line width structure for the 1, 2, 5, and 10 μm line width structures respectively. For each of these graphs, the curve fit shown in Figure 26 has been applied. For each graph, the points represent an individual LWS. All four LWSs (1, 2, 5, and 10 μm) of 6 to 8 DCRMSs were measured per wafer.

Figure 27 (1 μm LWS compared to the Optically Measured Line Width)

(Each point represents a 1 μm LWS. Multiple 1 μm LWSs were measured on multiple wafers)

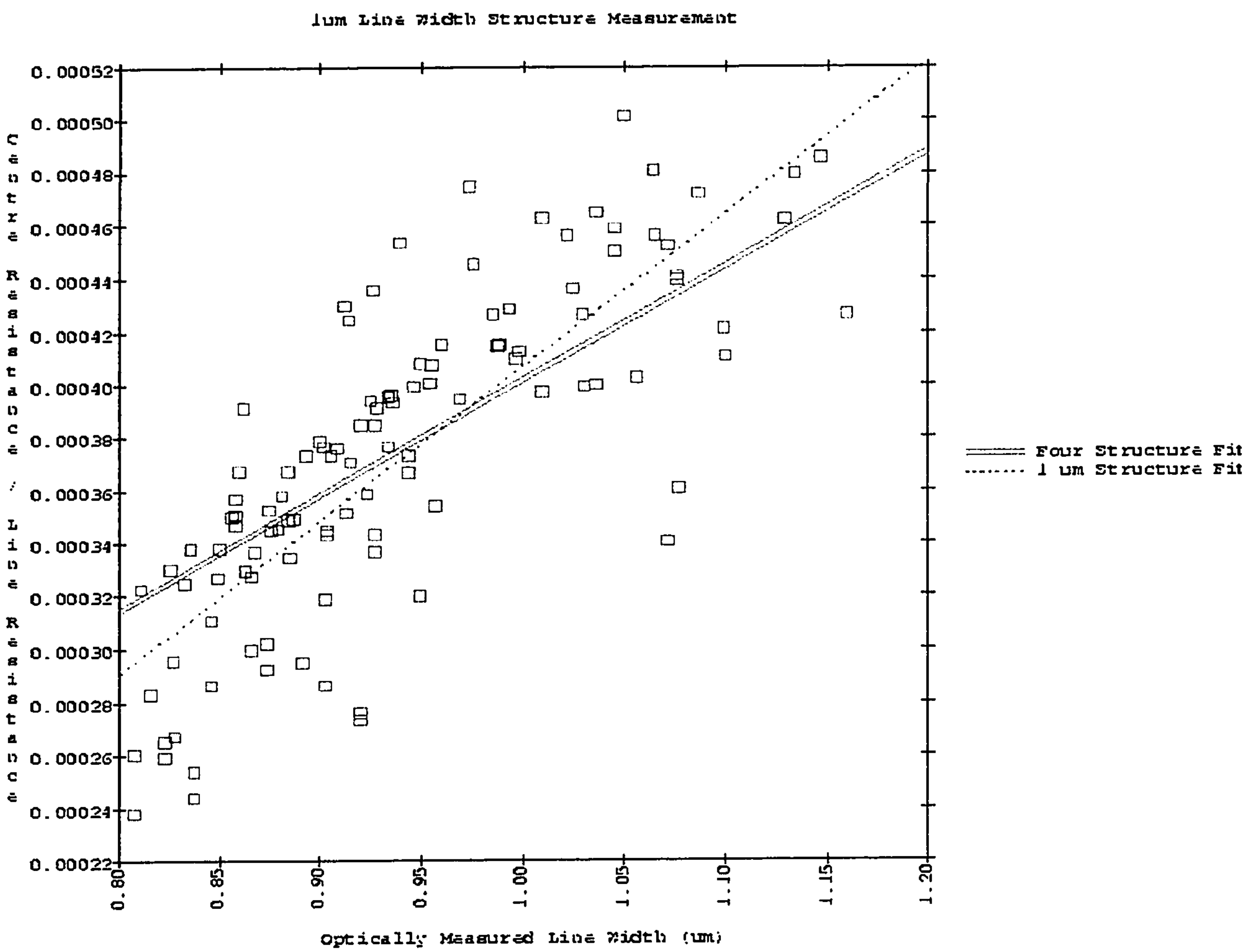

Figure 28 (2 μm LWS compared to the Optically Measured Line Width)

(Each point represents a 2 μm LWS. Multiple 2 μm LWSs were measured on multiple wafers)

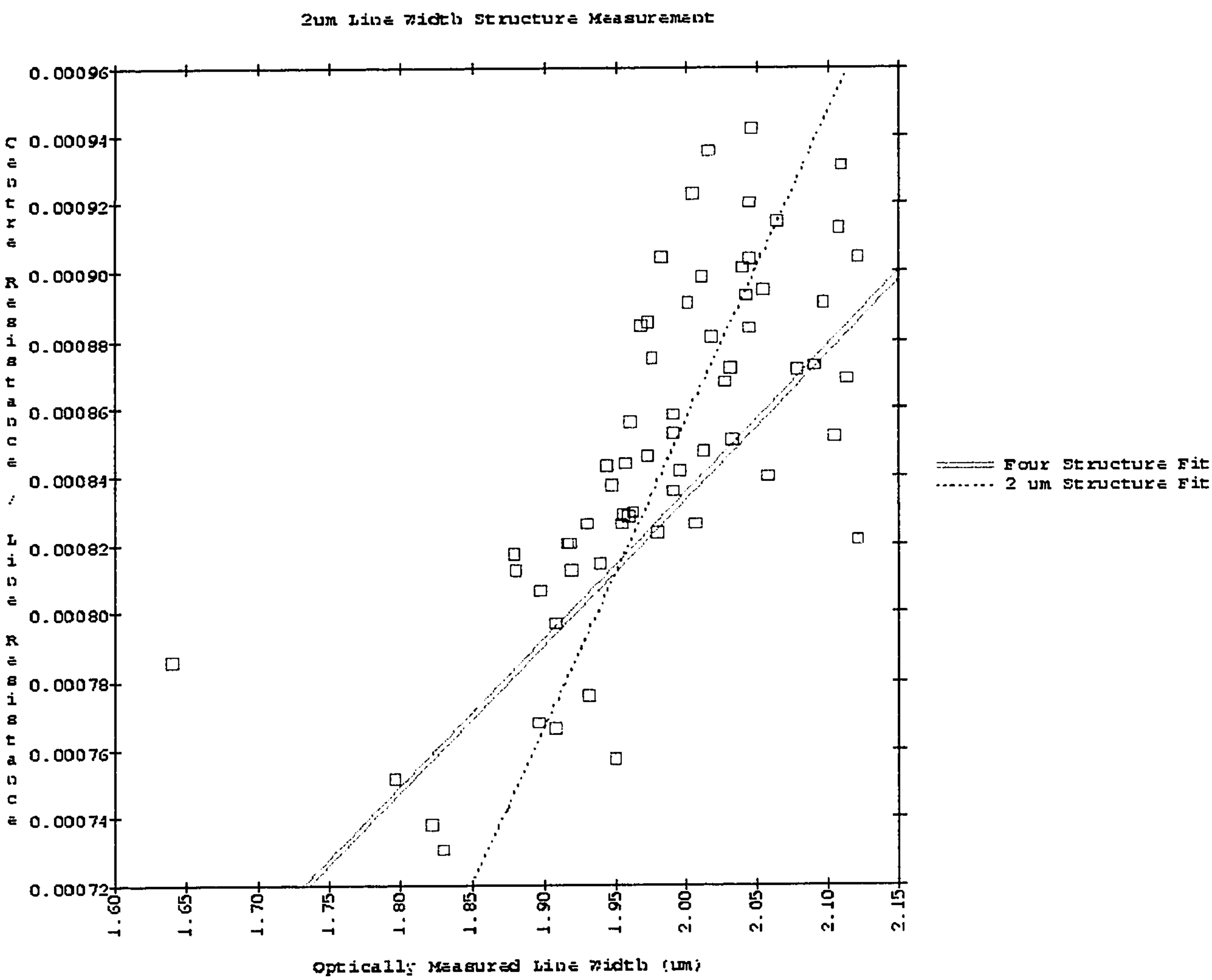

Figure 29 (5 μμ LWS compared to the Optically Measured Line Width)

(Each point represents a 5 μm LWS. Multiple 5 μm LWSs were measured on multiple wafers)

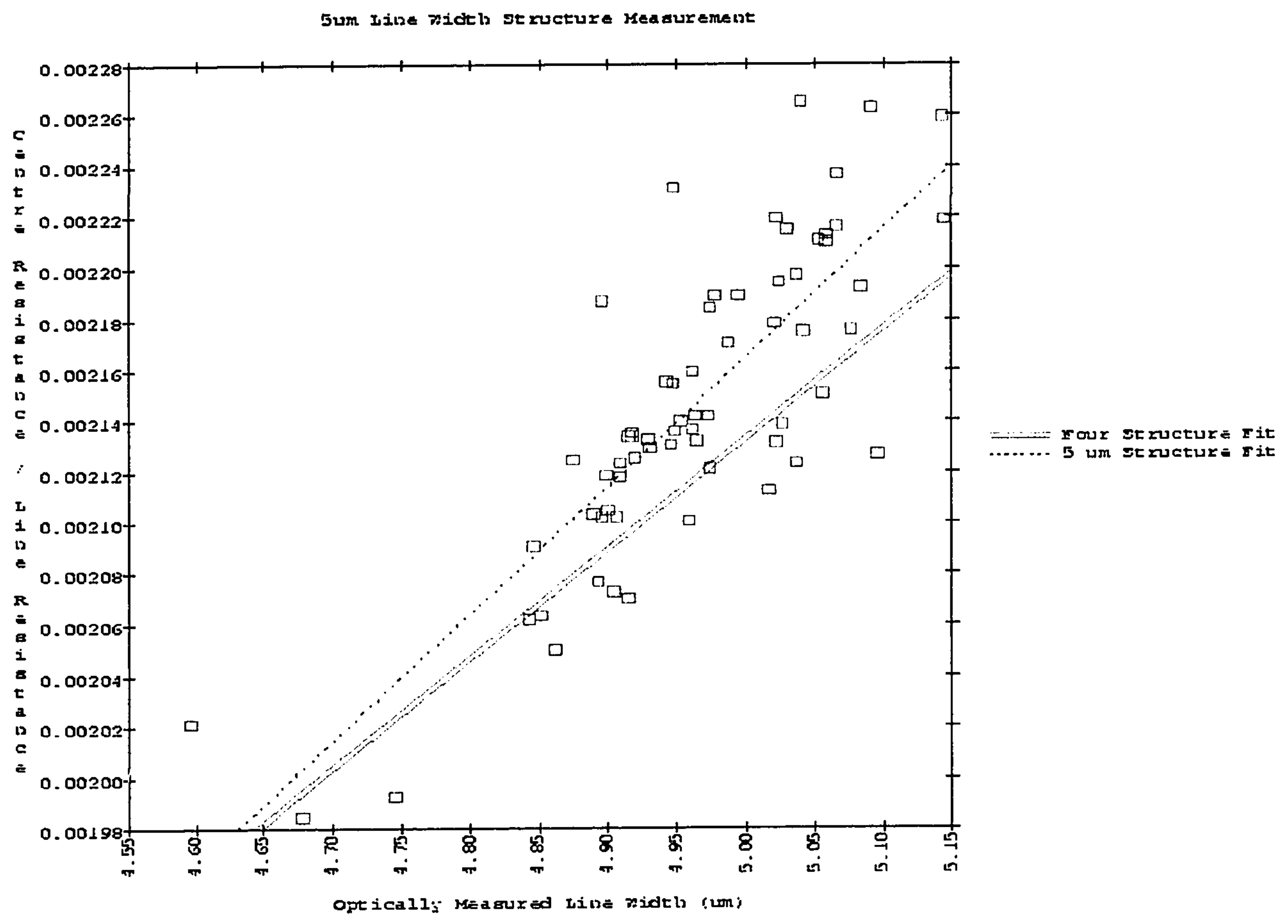

Figure 30 (10 μm LWS compared to the Optically Measured Line Width)

(Each point represents a 10 μm LWS. Multiple 10 μm LWSs were measured on multiple wafers)

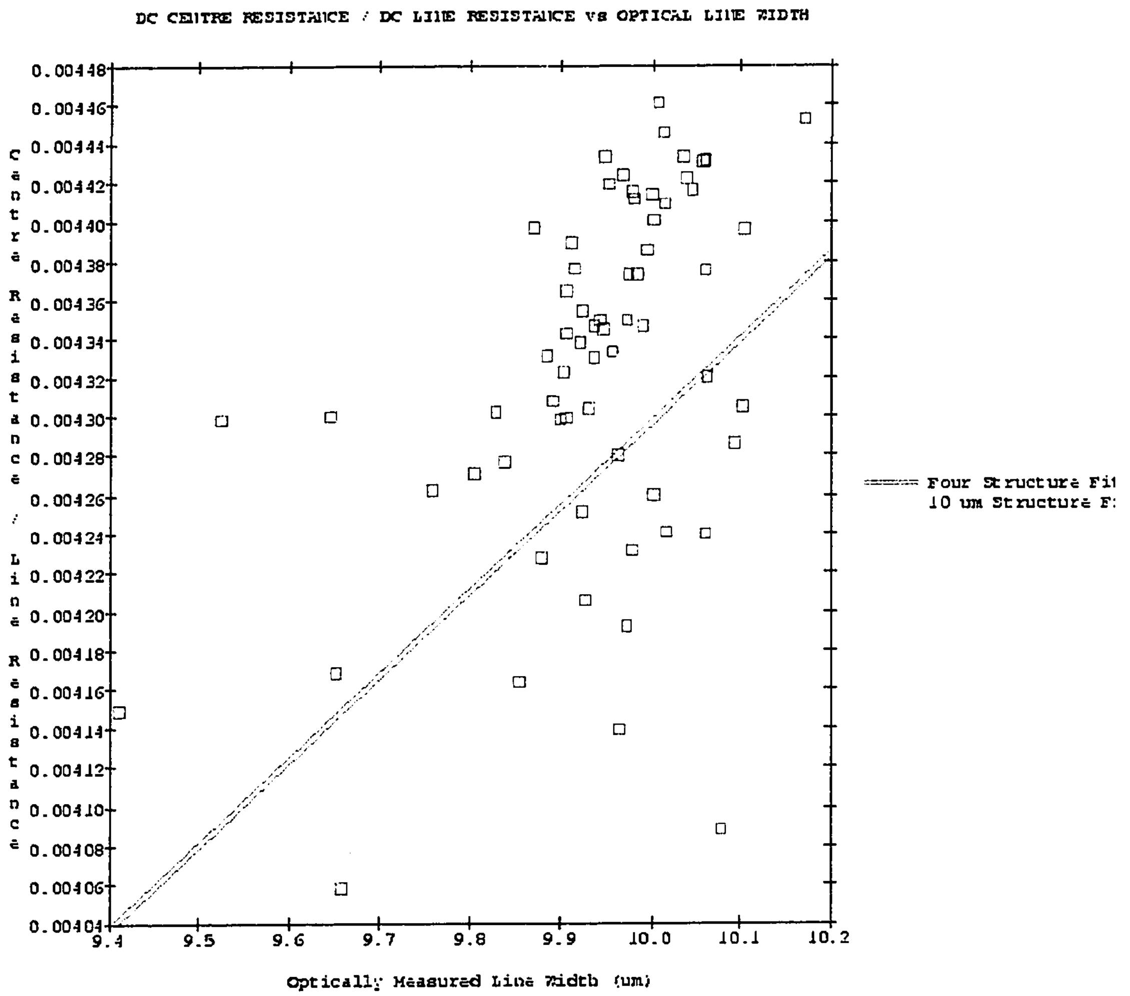

Looking at the 1μm line width structure (Figure 27), the distribution of data points does not fit the curve fit from Figure 26. A second line has been drawn fitting the data for the 1 μm line alone. The slope for the 1 μm line curve fit is larger than for the first curve fit. The points for the 2, 5, and 10 μm line structures in Figure 28, 29, and 30 respectively also have the original curve fit and the curve fit corresponding to the particular line width structure. The new curve fits are shown in Table 2. For all four line width structures, the curve fits for a particular LWS has a larger slope than that of a the curve fit for all the points. However, the slope for the overall line width fits in the uncertainty of the individual line width measurements. The y-intercept for all of the measurements except the 1 μm line) contains the y value of zero within the its uncertainty.

Table 2

Line Width	*Slope*	*Y-Intercept*
Overall	**(4.328 +- 0.212) e-04**	**-(0.310 +- 1.51) e-04**
1 um	**(5.806 +- 1.040) e-04**	**-(1.738+- 1.311) e-04**
2 um	**(11.07 +- 2.03) e-04**	**-(11.45 +- 17.40) e-04**
5 um	**(5.037 +- 1.102) e-04**	**-(3.542 +- 5.880) e-04**
10 um	**(8.680 +- 6.532) e-04**	**-(43.07 +- 52.84) e-04**

Since the curve fit for all three structures combined is a good fit, then the basic theory is correct. The optically measured line width against the SRS resistance / the LWS resistance (for the 1, 2, 5, and 10 μm structures together) is linear.

Even though the OSI measurements have +- 10% error for the 1 μm line, the same error is proportionally less for the larger lines. Therefore, if the slope differences were caused by errors in the optical measurements, the points would be more linear for the larger line width structures. By looking at Figure 30, it is obvious that this is untrue.

Therefore, the source of the error must be the division of the SRS resistance by the LWS resistance. Each resistance measurement is a source of error. By dividing one by the other, the error is magnified. The median value of the calculation of the SRS resistance over the LWS resistance value could give a good representation of the median value of the line width of a wafer. By taking the median, each wafer would have its large distribution averaged out. Taking the median value also eliminates the extreme values that can arise from dividing the resistance of the SRS by a very small LWS resistance value (if the error on the LWS resistance measurement results in a low LWS resistance value).

The errors themselves look random, as opposed to systematic. Ie. The error on the optical measurement seems to be independent of the error on the resistance measurement. The scattered distribution give credence to uncoupled errors between the two measurements. The source of the error on the resistance measurement is most likely different than the source of error on the optical measurement. This is supported by the method of measurement. The resistance method measure the entire volume of the line, while the optical method only measured a 2D slice of the line.

This hypothesis on the sources of error makes sense if the y values of Figure 30 are the source of the distribution of the data. The y values for Figure 30 have two sources error (SRS measurement and the LWS measurement) while the x values (optical measurements) have only one source of error. The exact cause of the measurement error for individual structures over all the structures combined will be better explained later when the quality of the dc centre measurement and the dc line width measurement structures are compared.

6.3.2 Verification of the SRS

The inverse of the dc centre structure resistance versus the mechanically measured metal thickness is shown in Figure 31. The curve fit argues the linear relationship between 1 / the resistance of the SRS and the metal thickness. In Figure 31, there are clusters of points. Each of these clusters corresponds to many sites measured on the same wafer or on wafers from the same metal deposition run. Notice that the distribution of points in each cluster is horizontal in nature. If the clusters were individually curve fitted, the slope of the points in each cluster would be far less than the slope of the overall curve fit. This suggests that there is a measurement error related to the x value of the points.

Figure 31 (Comparison of SRS Resistance to Mechanically Measured Metal Thickness)

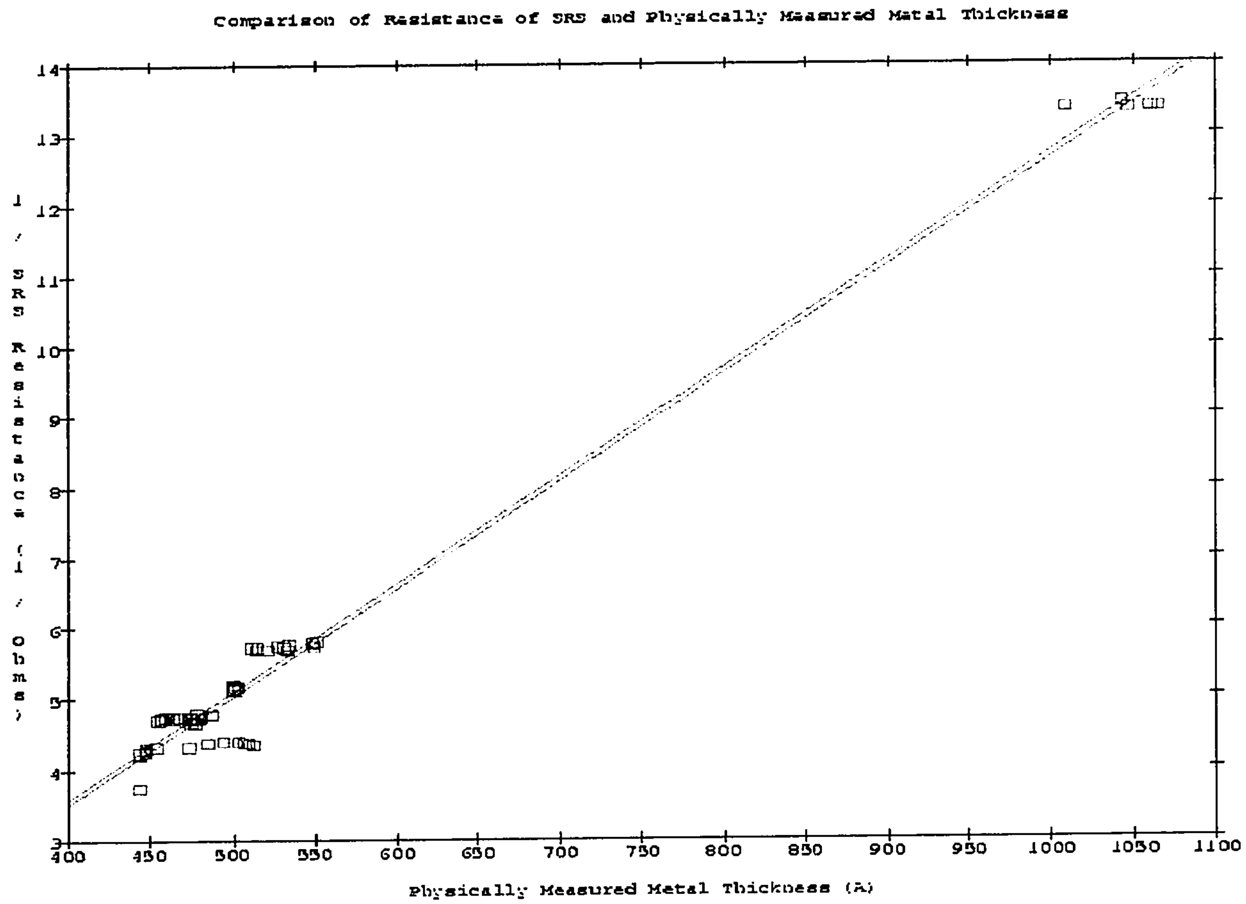

Therefore, there is an inherent error in the mechanically measured thickness. The larger of these clusters have a mechanically measured metal thickness variation range of 40 to 50 A. This gives a rough error in the surface profiled measurement of +- 20 to 25 A. The ionic radius of Al is 0.51 A. Therefore the physical measurement has an error of +- 20 to 25 Al atomic layers. Since the SRS is more representative of an average thickness (averages out roughness of the line), it is a more accurate measurement of the average thickness of the structure compared to a physical measurement at a point on a rough line.

It would appear that the SRS measurement is more accurate than the mechanically profiled measurement for measuring metal thickness. However, by being accurate to +-30 Al atomic layers, the mechanical measurement is still very accurate. The accuracy of the SRS equates to approximately +-5 A or +-5 Al atomic layers. The true test of the SRS is its accuracy in predicting the centre frequency of a SAW device.

6.4 Comparison of DCRMS to a SAW Device

With the basic relationship proven for all four LWSs and for the SRS, the next step was to apply the DCRMS to real SAW devices.

6.4.1 Design of DCRMS / SAW Device Experiment

The DCRMS were laid out on SAW device wafers as shown in Figure 32. There are five dc measurement sites. One at the centre and four at the edges, forming a cross. The objective was for the DCRMSs to be spaced to best statistically represent the distribution of SAW devices across a wafer.

The pattern seems to favour the outer edge of the wafer. However, the four of the five sites were chosen near the edge since the majority of die are near the edge (area of a circle is r^2).

At each dc measurement site, two complete DCRMSs were located. The remaining portion of each wafer was blanketed by SAW devices. Figure 33 is a photograph of one of the first run SAW device / DCRMS wafers. It does not have a complete set (pair) of DCRMSs at the top and bottom of the wafer. The wafers used for data collection in this paper did have DCRMS structures at the top and bottom of the wafers (as shown in Figure 32).

Figure 32 (Layout of DCRMSs on a Wafer of SAW Devices)

(The flat section at the bottom of the wafer is perpendicular to the direction of SAW propagation.)

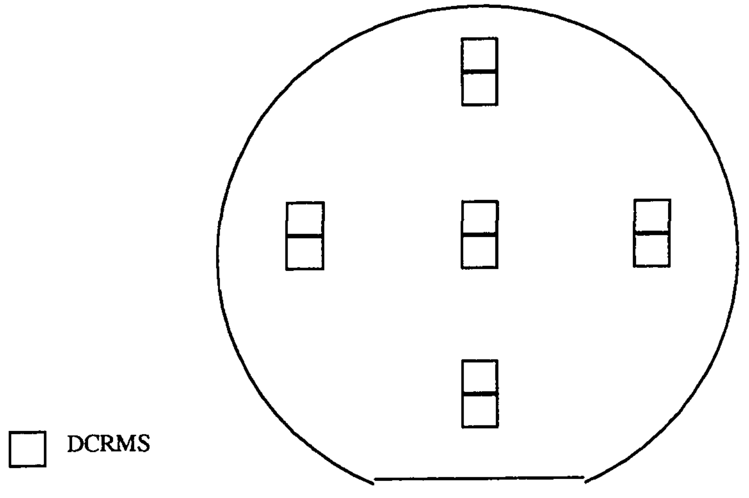

Figure 33 (Photograph of a Wafer of SAW Devices with DCRMSs)

(This is an example of DCRMSs laid out on a wafer of SAW devices. The white streak on the wafer is glare caused by the flash of the digital camera.)

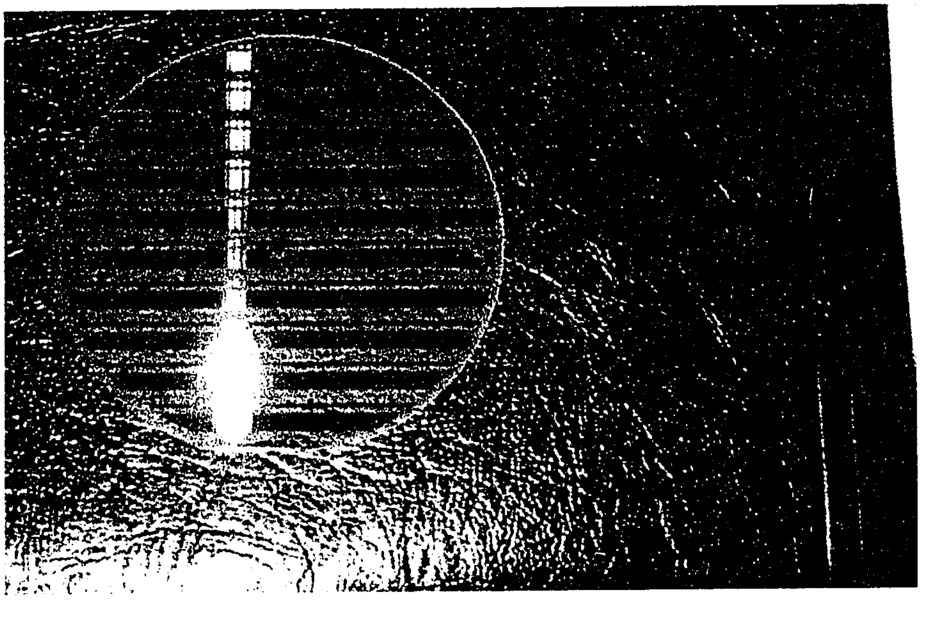

The wafers were processed in accordance with a 3 * 3 matrix of exposure energy versus metal thickness (Table 3). This would provide wafers exposed at three different exposure energies with three different metal thicknesses per exposure energy. The process split provides wafers with three different line widths with three different metal thicknesses per exposure energy.

Table 3 Layout of DCRMS/SAW Device Experiment (Exposure Energy and Metal Thickness)

Exposure	Metal Thickness		
	470A Al	500A Al	530A Al
180 mJ	wafer 1	wafer 4	wafer 7
200 mJ	wafer 2	wafer 5	wafer 8
220 mJ	wafer 3	wafer 6	wafer 9

The variations in metal thickness and exposure energy were chosen to replicate normal process variation in the fabrication of 500 A Al SAW devices.

6.4.2 Line Width and Exposure

The first step with the DCRMS / SAW device wafers was to establish the validity of the hypothesis that exposure energy affects the line widths of the DCRMS and SAW devices. Figure 34 shows the optically measured line width of the 1 μm LWS versus the exposure energy used to expose the photoresist.

Figure 34 (Effect of Variations in Exposure Energy on the 1 μm LWS)

(Each point is represents one 1μm LWS. The centre line of the LWS was measured. The points are taken from the LWS from three wafers at each exposure energy. Nine wafers in total.)

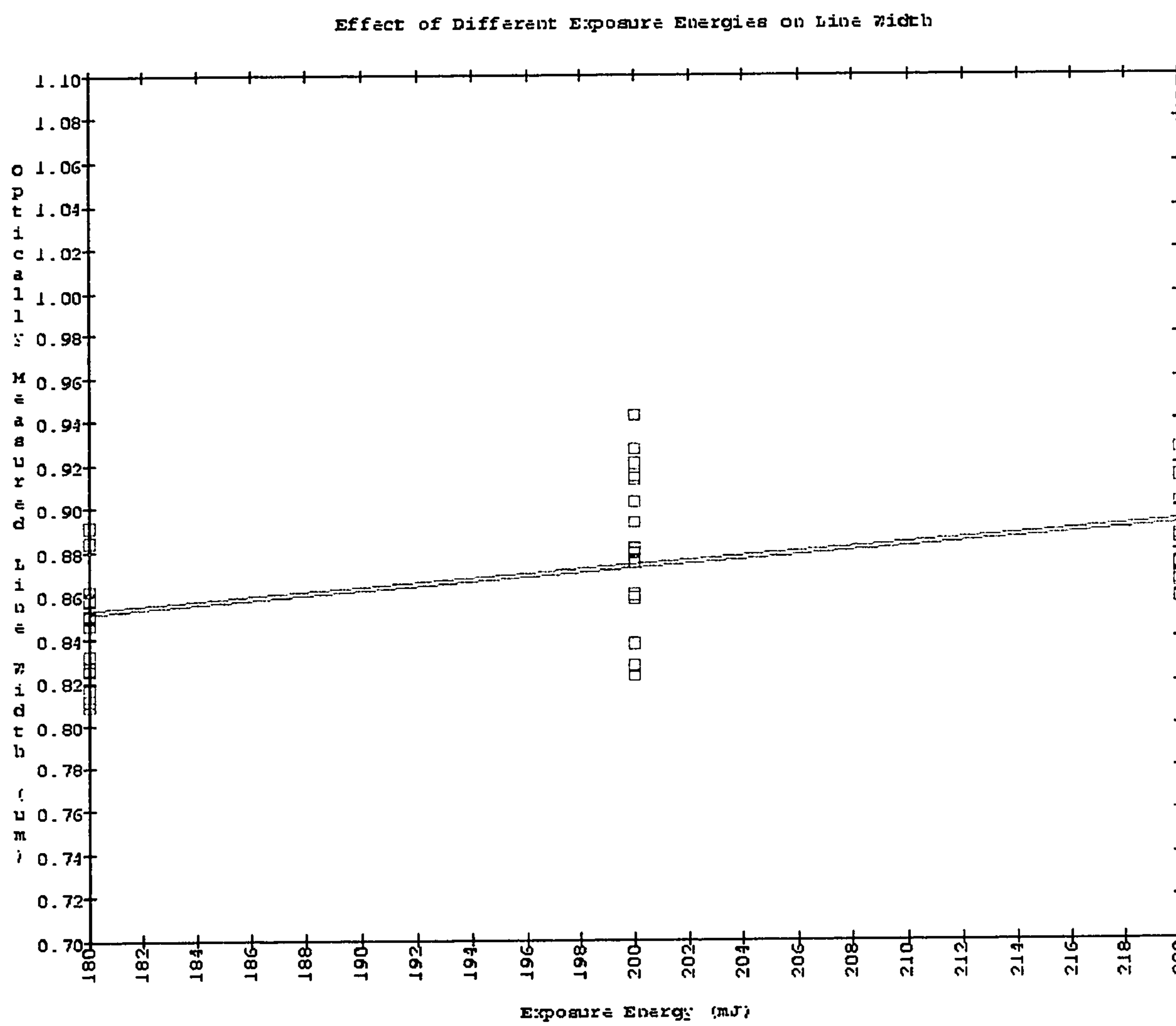

Even though there is a significant distribution of optically measured line width values for each exposure energy (roughly 10%), in general there is a 'linear' relationship between line width and exposure energy. As expected, the line width increases with increasing exposure (see Section 5.2). The large distribution in measured line width values for each exposure energy arises from the error in optically measuring optically line widths near 1 um.

In Section 6.3.1, the median value for a wafer of the SRS resistance over the LWS resistance was indicated as being an effective measure of the median line width of the wafer. From Figure 34, it would seem that the median optically measured line width has a linear relationship with exposure energy. Therefore, it would be fair to say that the median value of the line width, measured optically in at least 6 points on the wafers, is a good indication of the actual line width of the wafer.

For each exposure energy, 15 sites were measured. This reduces the measurement error of +-10% for a single measurement to an error of +-2.6% for the mean of these measurements. Using six sites, as described above, would reduce the error of the mean to +-4%, down from +-10% for a single measurement.

6.4.3 Centre Frequency

6.4.3.1 SRS and Centre Frequency

The centre frequency for all the SAW devices on each wafer of the DCRMS / SAW device experiment was measured. The thicknesses of all the SRSs on each wafer were measured mechanically. The resistance of each SRS on each wafer was measured.

Figure 35 shows the median centre frequency for each wafer plotted against the median mechanically measured SRS thickness. There is a strong linear relationship between the centre frequency of each device and the mechanically measured metal thickness. The slope of the linear relationship is roughly (4.8 +- 0.2) * 10^{-3} MHz / A (the error is chosen only from a curve fit of the 200 mJ exposure energy samples). Therefore the metallization causes a frequency shift of roughly 4.8 kHz per A of metal thickness. The y-intercept of this relationship is (841.284 +- 0.155) MHz . So the unmetallized SAW frequency would be near 841.284 MHz. The expected line width of the SAW device is 1.1 um. Therefore the wavelength of the SAW is 4.4 um. From the extrapolated unmetallized SAW frequency, the unmetalized surface velocity of the quartz is 3702 m/s.

Figure 35 (Comparison of Centre Frequency of the SAW Device to the Mechanically Measured Metal Thickness of the Centre Square of the SRS)

(Each point represents a single wafer. The centre frequency of all of the SAW devices on each wafer was measured. The metal thickness of the centre square of all 10 SRSs was measured.)

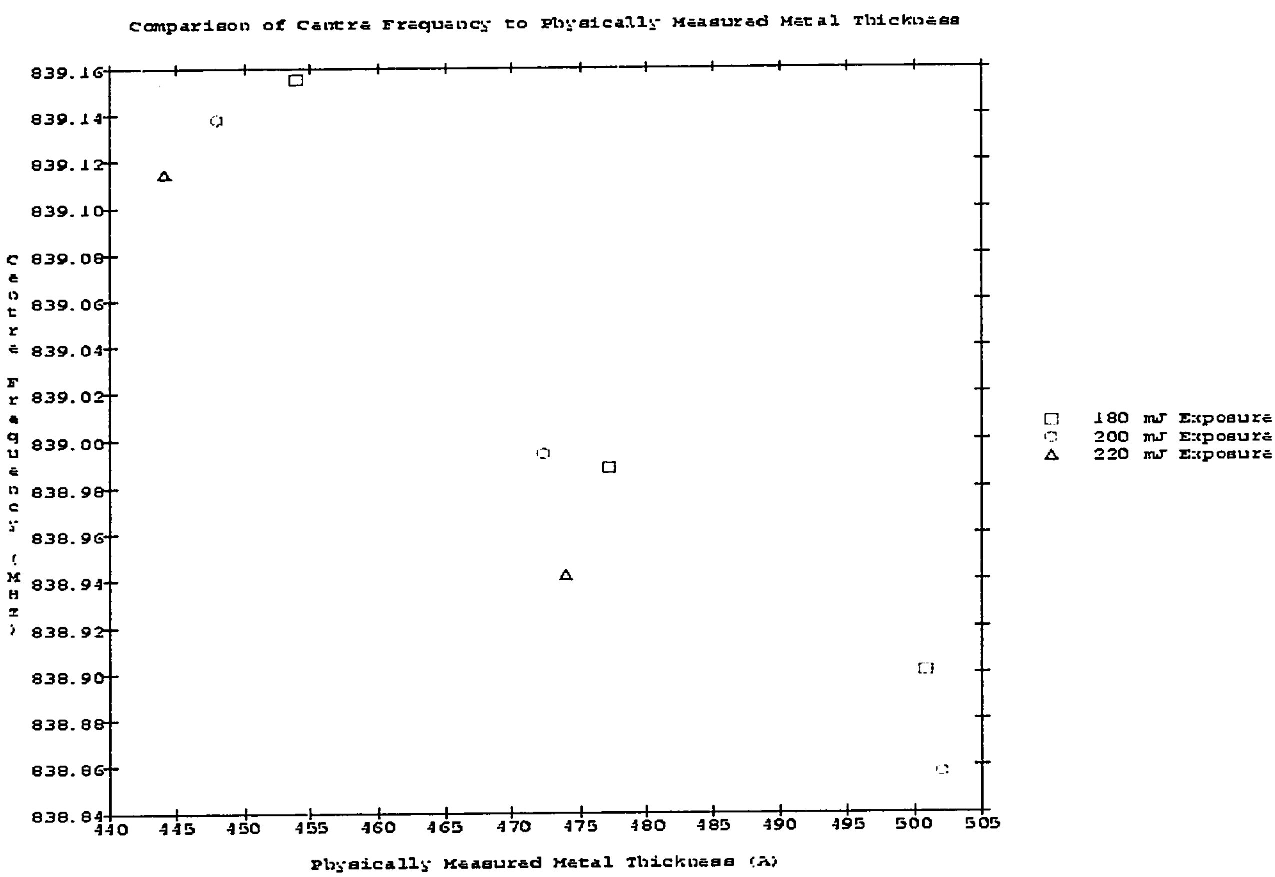

Figure 36 shows a graph of median centre frequency per wafer against median (dc resistance)$^{-1}$ of the SRSs per wafer. A curve fit of this plot gives a y-intercept of 840.266 MHz (3697 m/s). This curve fit differs from the plot against mechanically measured SRS thickness by 1.02 MHz (5 m/s). The published unmetalized surface velocity for 42 degree 45 minute ST quartz is 3158.8 m/s[30]. The cause of the discrepancy between the y-intercept calculated surface velocity and the published surface velocity is the fact that the linear relationship of velocity shift and metal thickness is only good as an approximation over short ranges of metal thickness. Over the range of 530 A to 0 A, the relationship is not completely linear. However, from Figure 35 and 36, the relationship is reasonably linear from 470 to 530 A.

30 Raytheon Research Division, "A Summary of SAW Properties for Several Useful Cuts of Quartz", PBN-91-2490f.

Figure 36 (Comparison of Centre Frequency of the SAW Device to DC Resistance of the SRS)

(Each point represents a single wafer. The centre frequency of all of the devices on each wafer was measured. The resistance of all 10 SRSs on each wafer was measured.)

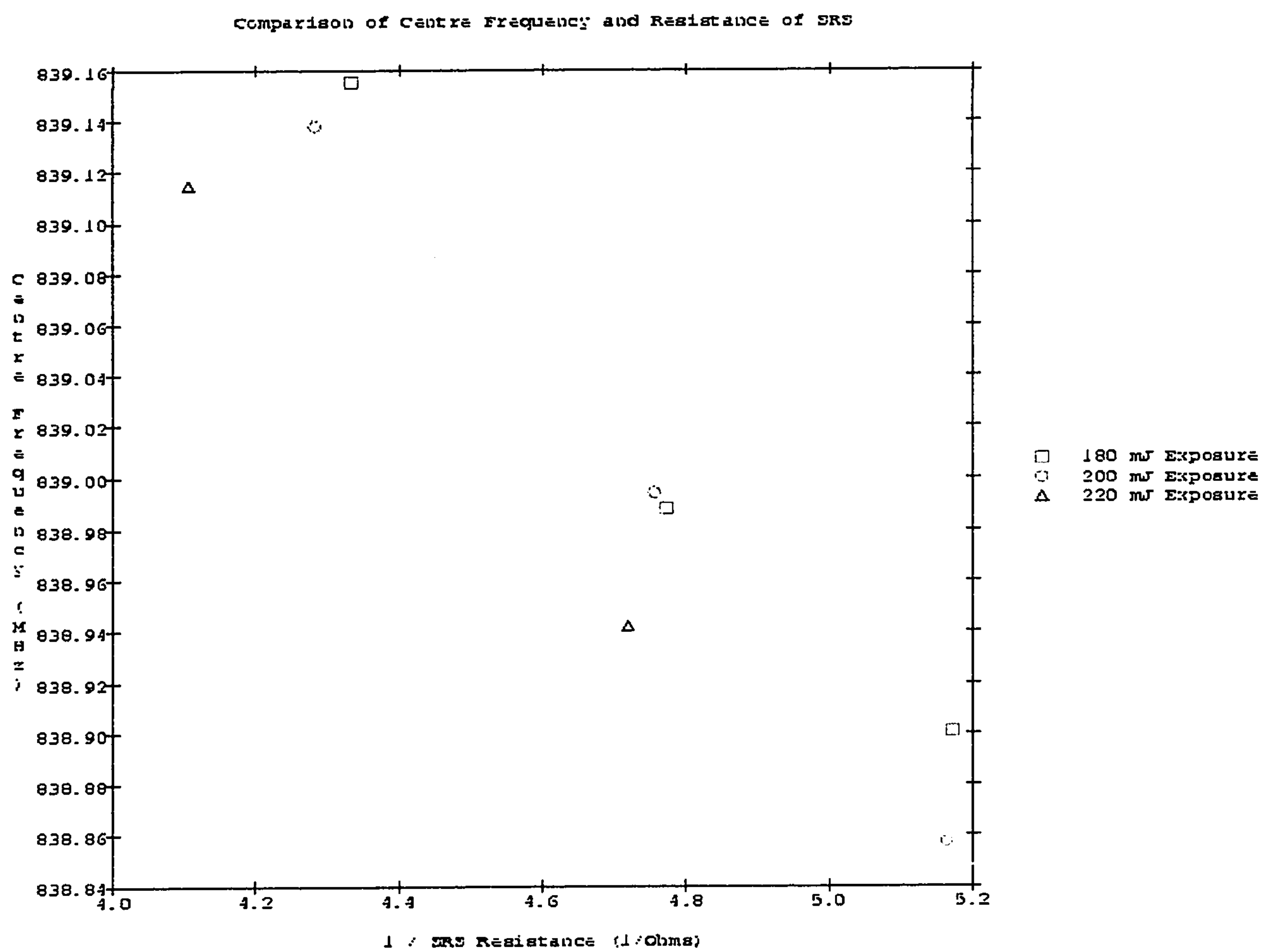

From Figure 36, there is a linear relationship between the 1 / SRS resistance and the centre frequency of the SAW device. From the graph, the median 1 / SRS resistance is accurate enough to determine the median centre frequency of this device within 0.02 MHz. The centre frequency tolerance (frequency range in which the SAW device has met its performance specification) of +-100 kHz from target is significantly larger than the SRS resolution of +-20 kHz. So, the SRS is effective in determining the basic frequency of this particular SAW device.

Also shown in Figure 36 is the exposure energy for each wafer (denoted by different symbols). For each of the three blocks of metal thicknesses, the highest frequency wafer had an exposure energy of 180mJ, the lowest frequency wafer has an exposure energy of 220 mJ, and the wafer with the centre frequency in the middle had an exposure energy of 200 mJ. The 220 mJ exposure wafer with target metal thickness of 530 A is not shown as it was broken in processing.

The 180 mJ wafer at a target aluminum metal thickness of 500 A, is slightly lower in frequency than the 200 mJ wafer as the same metal thickness. The cause of this discrepancy is most likely process related variation of the line width of that wafer. In other words, this wafer was affected by another stage of the fabrication process.

The ordering of the frequencies by exposure energy correlates well with theory. The lowest exposure energy should have the thinnest lines, and consequently the highest frequency. The highest exposure energy should have the widest lines, and therefore the lowest frequency.

The wafers at each metal thickness are distributed with the low line width wafers (square symbol) having the highest frequency for its metal thickness and the wide line width wafers (triangle symbol) having the lowest frequency. This verifies two things:

one, that line width is proportional to exposure energy; and two, that frequency seems to be proportional to line width.

Most importantly, the median value of the inverse of the DC resistance of the SRS has been proven to be very effective in determining the median centre frequency of the wafer.

6.4.3.2 One μm LWS and Centre Frequency

The centre frequency is proportional to the line width and the metal thickness; the line width is proportional to SRS resistance / LWS line resistance; the metal thickness is proportional to inverse of the SRS resistance. Therefore, the centre frequency of the device should be proportional to the inverse of the LWS line resistance. This assumes that the variation of the 1 μm LWS is proportional to the variation in the line widths of the 1.1 μm lines of the SAW device.

Figure 37 shows a plot of median centre frequency per wafer against the the inverse of the LWS resistance per wafer. There is a rough linear relationship between centre frequency of the SAW device to of the inverse of the LWS resistance. However, the relationship is very inaccurate. The main reason for this is the accumulated sources of error. The relationship between the variation of the 1 μm LWS line width and the variation of the 1.1 μm line of the SAW device is probably reasonably accurate, because the LWSs and the SAW devices are developed in the same method, under the same lens, and under the same conditions. However, as suggested in Section 6.3.1, the accuracy of the inverse of the LWS resistance may be poor.

Figure 37 (Comparison of Centre Frequency to the Inverse of the DC Resistance of the 1 μm LWS Structure)

(Each point represents a wafer. The centre frequency of all the SAW devices on each wafer was measured. The resistance of all 10 1μm LWSs on each wafer was measured.)

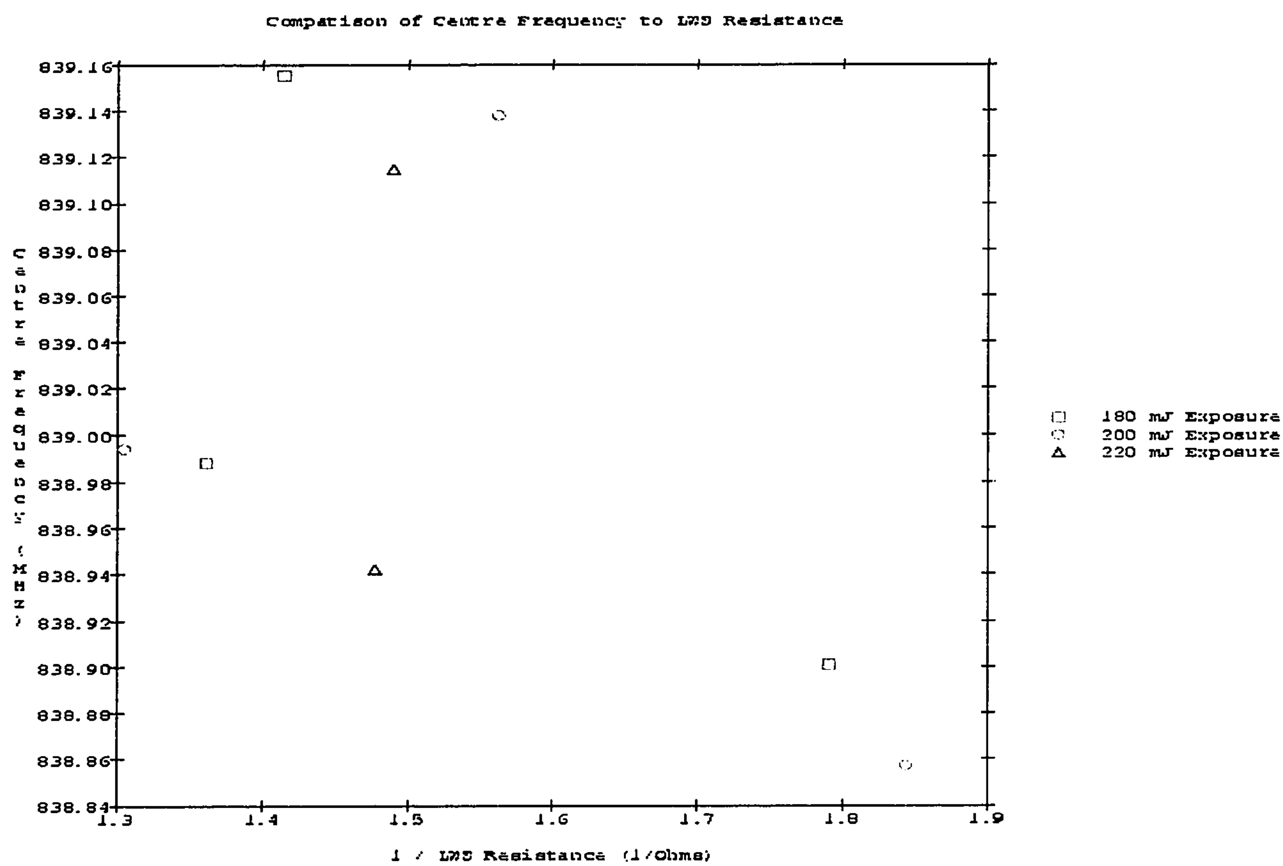

From Figure 37, it does not seem that the 1 μm LWS is very effective for determining the centre frequency of the SAW device. From the scattering of points about the linear curve fit in Figure 27, it does not seem that the 1 μm LWS resistance measurement is very effective for determining the line width of the LWS. It would not be avisable to trust millions of dollars of SAW device production to the scant correlations shown in Figures 27 and 37.

6.4.4 Bandwidth

6.4.4.1 Bandwidth and Exposure Energy

With most SAW devices, variations in line width result in variation in bandwidths of the transmission response of the devices. With the variation in exposures, the line widths of the SAW devices and of the LWSs varied.

Figure 38 shows a graph of the median bandwidth (per wafer) of the SAW device against exposure energy. From Figure 38, a linear relationship is observed between exposure energy and bandwidth within the range of 180 mJ and 220 mJ exposure energy. Since exposure energy and line width seem to be linearly related, this suggests that bandwidth has a linear relation with line width.

Figure 38 (Bandwidth and Exposure Energy)

(Each point represents a wafer. The bandwidth of all the SAW devices on each wafer was measured.)

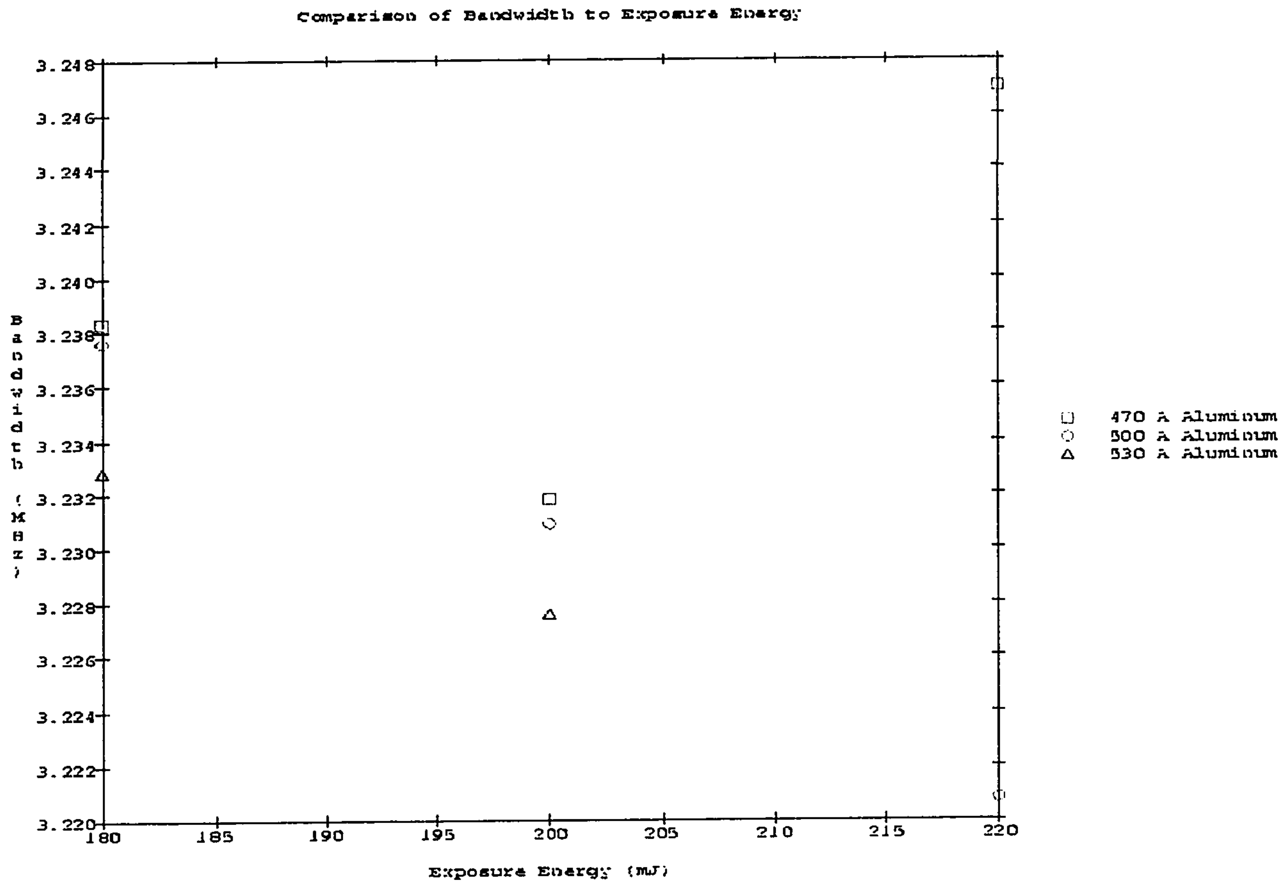

There is some variation in bandwidth at each exposure energy. Figure 38 has different symbols for wafers with different target metal thicknesses. Figure 38 shows that bandwidth is also related (to a lesser degree) to metal thickness. The greater the Al thickness, the smaller the bandwidth.

6.4.4.2 Bandwidth and Optically Measured Line Width

The linear relationship between median bandwidth and exposure energy suggests a linear relationship between median bandwidth and the line width of the 1 μm LWS (since the SAW device has line widths close to 1 um). With a variation in the line width of the 1 μm LWS there should be a corresponding variation in line width of the SAW device.

Figure 39 shows a graph of median bandwidth (per wafer) against the median optically measured line width of the 1 μm LWS (per wafer). A linear relationship is observed between the median bandwidth of the SAW devices and the line widths of the 1 μm LWS. However, the data points are significantly dispersed. In general, the relationship looks good, but the uncertainty in the optical line width measurement tool clouds the relationship.

Figure 39 (Comparison of Bandwidth of SAW Devices to the Optically Measured Line Width)

(Each point represents a single wafer. The bandwidth for all of the SAW devices on each wafer was measured. The optically measured line width of the centre line of all of the 1 μm LWS on the wafer was measured.)

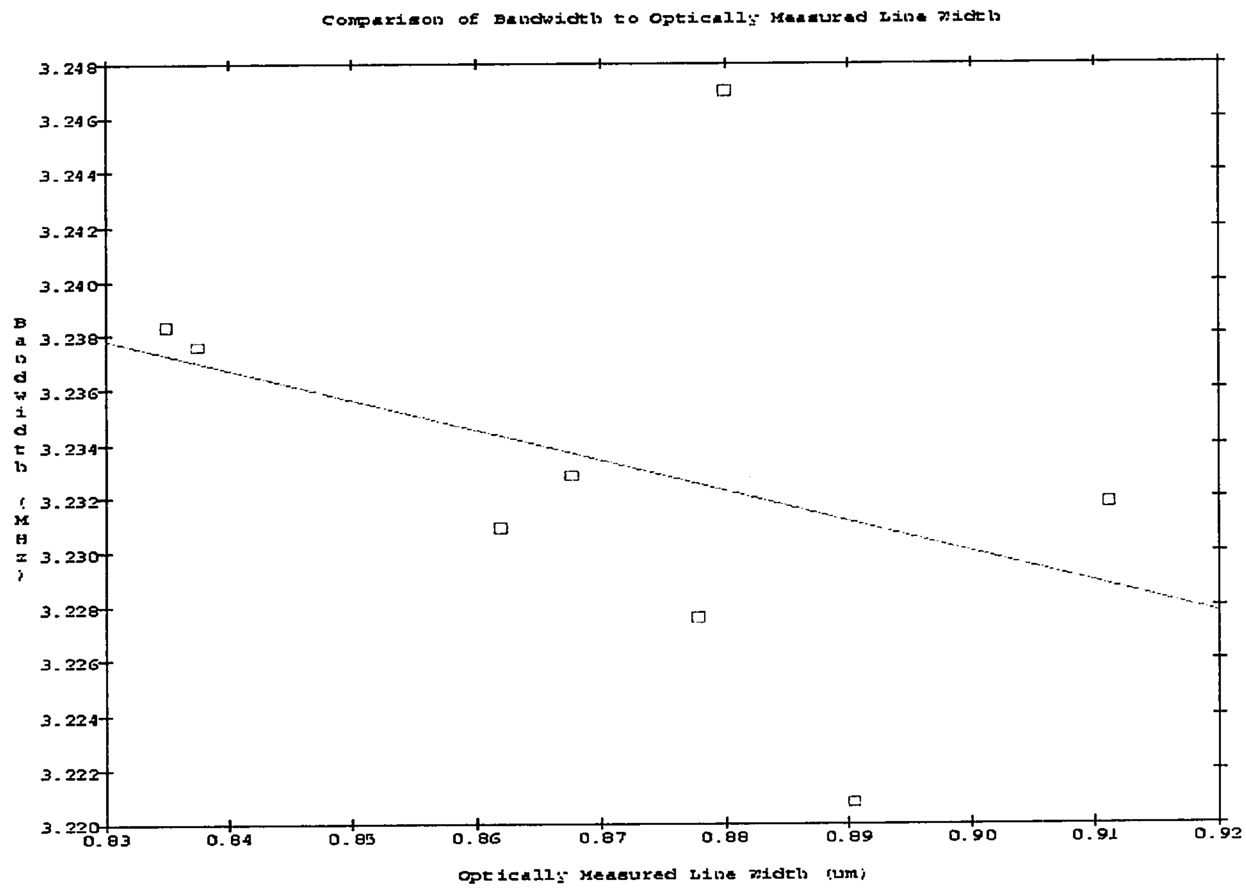

The data suggests that there is a relationship between the bandwidth of the SAW device and the optically measured line width of the 1 μm LWS; however there is a need for more data points to substantiate this claim. If the wafer with a bandwidth of 3.247 MHz and measured line width of ~0.88 μm was eliminated from Figure 39, then the data would have a reasonably linear relationship. However, with so few data points, none of the points can be removed without cause.

Even without a perfectly linear relationship, the optical measurements do suggest a relationship between bandwidth and the 1 μm LWS.

6.4.4.3 Bandwidth and the Resistance of the 1 μm LWS

Figure 40 shows the graph of the median bandwidth (per wafer) of the SAW device on a wafer against the resistance of the SRS / the resistance of the 1 μm LWS.

Figure 40 (Comparison of Bandwidth of SAW Devices to the DC Resistance of the SRS / the DC Resistance of the 1 μm LWS)

(Each point represents a single wafer. The bandwidth for all of the SAW devices on each wafer was measured. The resistances of each SRS / 1 μm LWS pair for all of the 10 DCRMS per wafer were measured. Values shown here are the median values for each wafer. The median SRS resistance / 1 μm LWS resistance is the median of the 10 calculated values of the (SRS resistance / 1 μm LWS resistance) for each wafer)

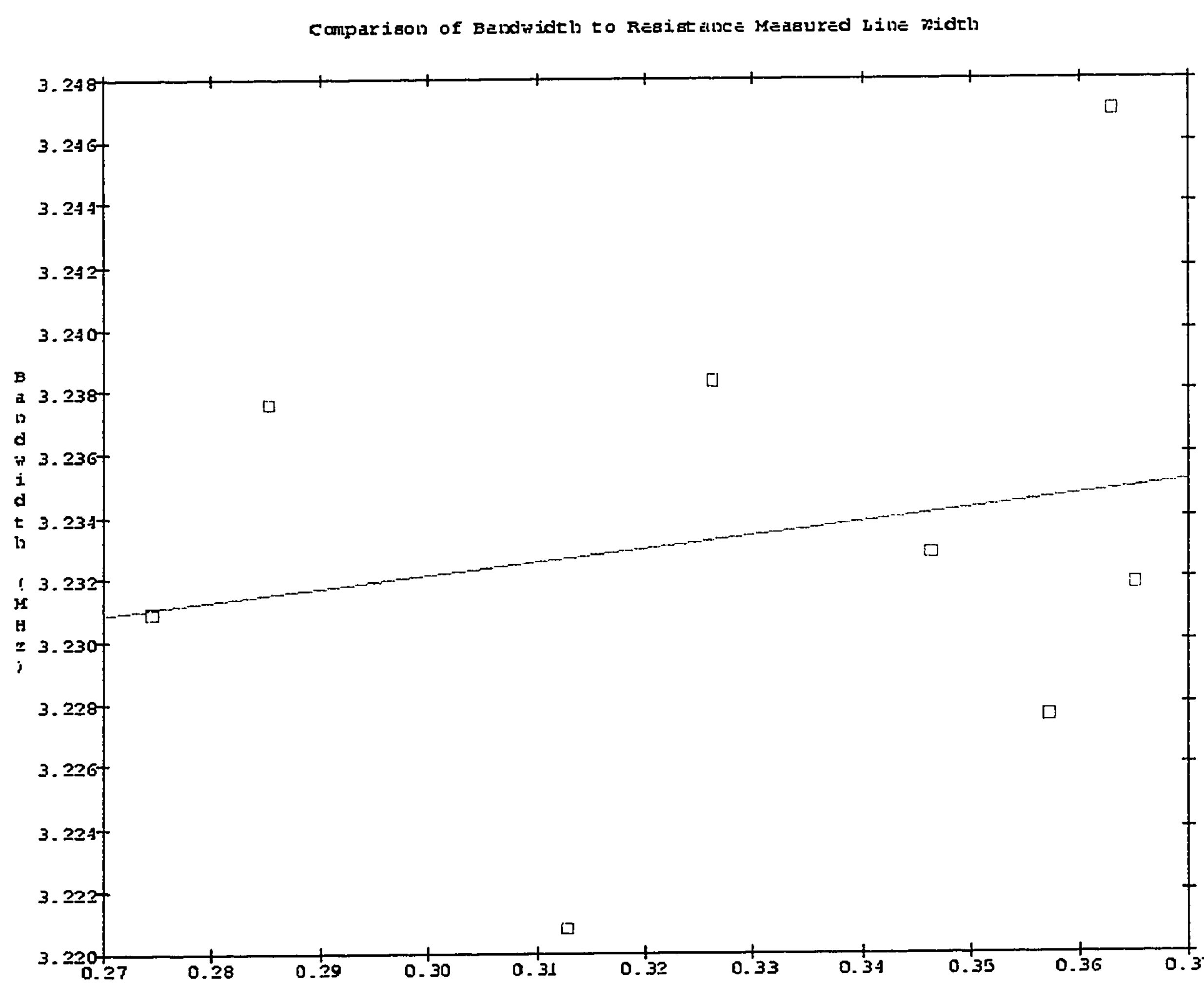

No correlation can be seen between the bandwidth of the SAW device and the resistance of the 1 μm LWS. The line drawn in the graph is a linear regression plot of the data. This line was added, not to demonstrate correlation, but to show how far the data points are from a linear correlation. This lack of correlation is probably due to the uncertainty in the resistance measurement of the LWS, rather than because of a lack of correlation between line width and bandwidth.

7.0 Conclusion

The equipment used as control monitors for the DCRMS measurements were not as accurate as desired, however the were acceptable tools. The DCRMS was effective in measuring metal thickness, but not effective in measuring small changes in line width. Centre frequency correlated well to the SRS measurements, but not the LWS measurements. Bandwidth did not correlate particularly well with either the SRS or LWS measurements.

The profiling thickness measurement tool was fairly accurate in measuring variation in metal thickness of Al lines at 450 to 1000 A. The mechanical measurements were off by ~40 A from the SEM measurements of the same structures. However these tools seemed capable of measuring metal thickness variation and were acceptable to use as a reference for the SRS.

The optical measurement of line width under 1 µm seemed barely adequate. The optical measurements were similar to SEM measurements of the same metal lines, but with less accuracy. It was hardly acceptable as an accurate reference for the LWS, but was the only tool available.

The SRSs obeyed Ohm's law for Al thickness of 450 A to 1000 A, as there was a linear relationship between physically measured Al thickness and 1 / the SRS resistance.

The LWSs also obeyed Ohm's law. There was a linear relationship between the line width of the LWS and the resistance of the SRS / the resistance of the LWS. However, this was only truly accurate when plotting the four LWS types (1, 2, 5, and 10 µm) on the same graph. The relationship for each individual LWS had a significant distribution of SRS resistance / LWS resistance for a range of optical line width measurements.

The main cause of this variation was the accumulated error involved in dividing the resistance of the SRS by the resistance of the LWS. The error in the SRS measurement would be independent of the error on the LWS measurement. The two structure measures independent shapes. The LWS would be susceptible to minor damage in the measurement line, while the sheet resistance square pad of the SRS would not.

Variations of exposure energy led to variations in centre frequency of the SAW device and variations in bandwidth of the SAW device. Variations in metal thickness also led to variations in centre frequency and bandwidth.

The variations in metal thickness were the main causes of the variations in the centre frequency of the SAW device. The variations in exposure energy (and therefore line width) only had a minor effect on centre frequency. The variations in exposure energy were the main cause of variation in bandwidth of the SAW device, while the variation in metal thickness only had a minor effect on the bandwidth of the SAW device.

The SRS resistance / the LWS resistance was related to the optically measured line width. For each particular LWS, the SRS resistance / the LWS resistance was less accurate than the optically measured line width. When taking into account all four LWSs at once, there is a strong linear relationship between SRS resistance / LWS resistance and line width. However, there is a relatively large distribution of values of the SRS resistance / the LWS resistance for a particular LWS compared to the overall linear relationship of all four structures.

The LWS was not an accurate device for measuring line width. However, neither was the optical measurement tool at small line widths (1 μm and lower).

The inverse of the 1 μm LWS resistance was ineffective for determining the centre frequency of the SAW device. There was no strong correlation between the inverse of the 1μm LWS resistance and centre frequency of the SAW device.

There was no strong correlation between the SRS resistance / the LWS resistance and the bandwidth. From the exposure energy and bandwidth results, it was clear that line width has an effect on bandwidth. The low correlation between the SRS resistance / LWS resistance and bandwidth provides more evidence that the DCRMS does not accurately measure line width.

Most correlations involving the LWS were ineffective. The LWS produced results that agreed with Ohm's Law; however, measuring the resistance of the LWS was not useful in resolving the variation in line width of the LWS or related SAW devices. Even though the optical line width measurement tool was not very accurate below 1 um, the 1 μm LWS was less effective at measuring line width.

One reason for the inaccuracy of the 1 μm LWS is the variations in the lens of the lithographic equipment. The pattern is not just blindly exposed onto the photoresist. There is a high quality optical lens that focuses the pattern onto the surface of the wafer. In a well controlled process, variations in the line widths across the wafer are very small. In this paper, observed variations were under 0.1 um, well below the wavelength of visible light.

Small defects in the lens can lead to a variation of focus across the wafer. Since the LWS is not exposed in the same portion of the lenses as the SAW devices, the lines of the SAW devices will be focused slightly differently. These lens are of very high quality (and value), so this variation is very small (under 0.1 um), but this is the magnitude of line width the LWS is attempting to detect. However, such variations could indirectly explain the inaccuracy of the LWS in predicting the centre frequency and bandwidth of the SAW devices on the wafer.

The second reason for the inaccuracy of the 1 µm LWS, was defects in the line structure itself. Figure 41 shows a SEM view of the 1 µm line of the 1 µm LWS. Notice the 'mouse bites' out of the side of the 1 µm line. The LWS resistance is inversely proportional to the mass of the line. With sections of the line missing, the actual mass of the line would be smaller. The number of sections of the line missing would be variable and would account for the large variations in the resistance of the LWS. The 'mouse bites' would be related to problems with the mask used to expose the LWS. Since the optical measurement is conducted at one spot on the line, chances are the measurement would avoid most of the mouse bites. The variation in this controlled experiment caused by exposure were at most 0.02 µm or 2% of the mass of the line. This value is taken from the linear regression of the medians of the optically measured line width. With the error from optical measurement tool for line widths near 1 um, the median value of each exposure energy is far more accurate than the individual points. The variation caused by the 'mouse bites' can be up to 5% of the mass of the line. This is 5% within a wafer, while the exposure energy variation would only be 2% between wafers of different exposure energy. Within a wafer of single exposure energy, the error should be much smaller. This report does not provide any quantitative results for the line width variation in a wafer caused by variation in exposure energy across the wafer.

The mask used for the SAW device is a different mask than for the DCRMS, and did not have a problem with 'mouse bites'. The change in mass of the 1 μm LWS would not be reflected by the same proportional change of line width by the SAW device. Therefore, the centre frequency and bandwidth of the SAW device would not vary due to 'mouse bites' while the resistance of the 1 μm LWS would.

Figure 41 (Defects in the Central Line of the LWS)

(The two crosses are displayed on each side of a the centre measurement line of the 1 µm LWS.)

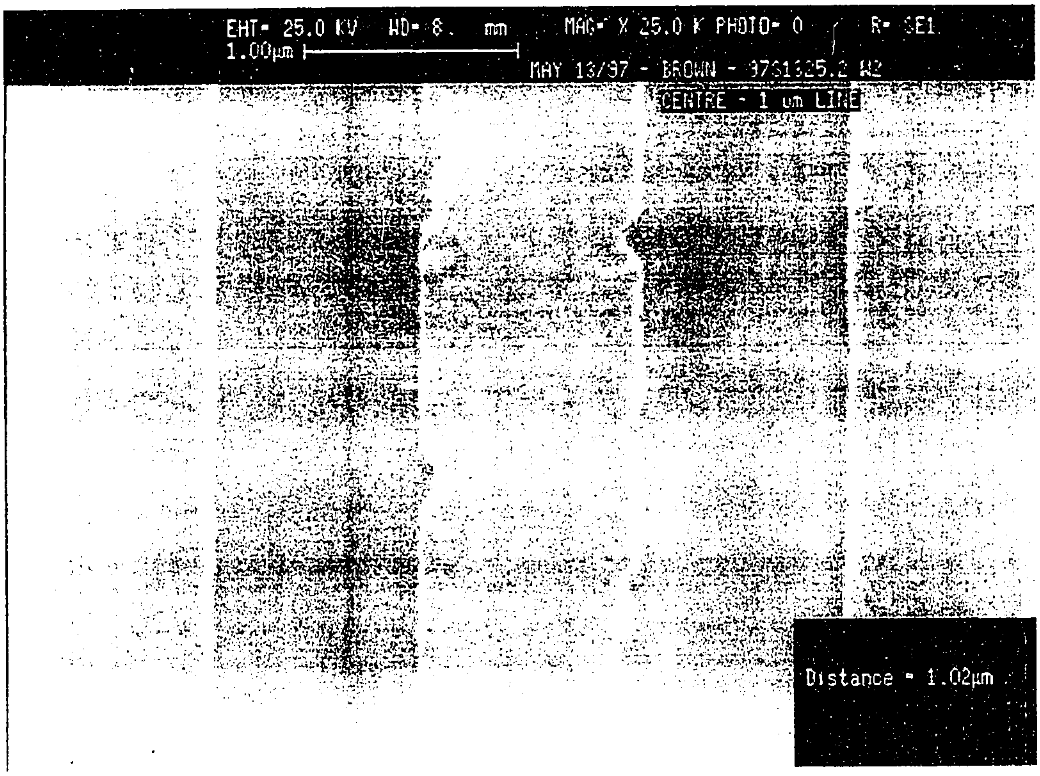

The 'mouse bites' were randomly seen on all four types of LWSs. This could account for some of the problems with correlating the LWS structures to optically measured line width and electrical properties (centre frequency and bandwidth) of the SAW device. A new mask for the DCRMSs would have to be fabricated to re-correlate the resistance of the LWSs to the measured line width. However, even accounting for the mouse bites, the resistance of the LWS looks like a poor tool to monitor line width variation and SAW device performance variation. Even though the LWS would be poor at monitoring minor variations in the line width, the LWS would probably be effective in determining large line width variation caused by other process problems (large changes in resist thickness or developing of exposed areas). The optical measurement would also be effective in detecting these large changes. However, the LWS has the advantage of being easily automated and therefore, faster.

Moreover, before condemning the accuracy of the LWS, it should be said that the method of line width variation all created the smallest of change. For all of the line width measurement types (the optical line width measurement, the LWS, and the SAW device measurements), only the SAW device measurements detected any tangible effect of line width variation. Figure 34 only shows the smallest change in average optically measured line width.

The LWS do not seem accurate enough to measure very small deviation in line widths, but should still be effective in determining large line width variations. The line width variation simulated in this thesis were smaller than the magnitude of line width variation necessary to cause failure of SAW devices.

The mechanically measured metal thickness correlated well to the inverse of the resistance of the SRS. From the data, the uncertainty in the value of 1 / the SRS resistance is smaller than the uncertainty in the mechanically measured metal thickness.

The centre frequency of the SAW devices correlated well to the inverse of the resistance of the SRS. By taking the median of 1 / the resistance of the SRS for a wafer, the median centre frequency of the wafer could be predicted within 0.02 MHz. This is significantly more accurate than predictions based on the physical measurement of the metal thickness. For SAW devices that cannot be measured in die form, the SRS would be an effective structure for determining the median centre frequency of the SAW devices on a wafer.

Since the SRS is more accurate than the mechanical measurement of the metal thickness, the SRS would be an effective process control monitor. If a wafer was blanketed (fully covered) with SRSs then intra-wafer metal uniformity could be monitored within a high degree of accuracy.

The LWS was less accurate in measuring small change in line width in of SAW devices. The accuracy of the 1 μm LWS was not good enough to predict the frequency response of a SAW device with 1.1 μm line widths on the same wafer. A more accurate measurement structure would be a simple SAW device, that could be measured on the wafer, and was extremely sensitive to line width variation. The network analyzer is an extremely accurate measurement tool and could make very high precision measurements of the simple SAW device.

In the end, four simple SAW devices could replace the four LWS structures. The four SAW devices could be constructed to be properly matched when probed on the wafer (they do not need to be matched to a final system or usage). A SRS structure in conjunction with a simple SAW device would provide a more accurate view of variation in metal thickness and line width. The SRS structure would monitor metal thickness variation. From the metal thickness variation extrapolated from the SRS resistance measurement, the effect of metal thickness variation on the simple SAW device could be normalized out. This would leave the resulting centre frequency variation completely dependent on variation in line widths of the simple SAW device.

In short, the SRS portion of the DCRMS is a success. It has proven to be an effective monitor of metal thickness variation. The LWS portion of the DCRMS was not a success. The lack of accuracy of the LWS does not lend itself to be a worthwhile process monitor of line width variation.

Appendix A

Abbreviations

DC	- Direct Current
DCRMS	- Direct Current Resistance Measurement Structure
Fc	- Centre Frequency
IDT	- Interdigital Transducer
IF	- Intermediate Frequency
LWS	- Line Width Structure
RF	- Radio Frequency
SAW	- Surface Acoustic Wave
SEM	- Scanning Electron Microscope
SRS	- Sheet Resistance Structure

Appendix B

Terms

Bandpass filter

A device that filters all frequencies of a signal except those within a particular range of frequencies.

Bandwidth

The bandwidth of a bandpass filter is the frequency range contained at a specified amplitude below the maximum attenuation of the bandpass curve. (This concept is generally denoted in the form "bandwidth at −2 dB". Where −2 dB is the specified attenuation below the point of maximum attenuation.

Bus Bars

The metal pads perpendicular to the metal lines, attached to the metal lines. These bars are usually the point of contact for wire bonds and contact probes.

Centre Frequency*

Arithmetic mean of the cut-off frequencies.

Cut-off Frequency*

A frequency of the pass band at which the relative attenuation reaches a specified value.

Direct Current Resistance Measurement Structure

A single layer metal structure consisting of a centre sheet resistance structure and four line width structures.

Fingers

Another term for the metal lines of an interdigital tranducer.

Insertion Loss

The point of maximum amplitude of transmission for a bandpass filter.

Interdigital Transducer*

A SAW transducer made of a comb-like conductive structure deposited on a piezoelectric substrate transforming electrical energy into acoustic energy or vice versa.

Intermediate Frequency

The intermediate frequency of a wireless radio. In this paper, this refers to frequencies from 80 to 220 MHz.

Line Width

The width of the metal line of an interdigital transducer of a SAW device or of the critical line (central line) of a line width structure.

Line Width Structure

A single layer metal structure used, in conjunction with an attached sheet resistance structure, use to measure the line width of a metal line. Based on the bridge structure.

Pass Band*

A band of frequencies in which the relative attenuation is equal to or less than a specified value.

Radio Frequency

The transmission or reception frequency of a wireless radio. In this paper, this refers to frequencies around 880 MHz.

Sheet Resistance Structure

A single layer metal structure used to measure the sheet resistance of a layer of deposited metal. Based on the van der Pauw sheet resistance structure.

Surface Acoustic Wave*

An acoustic wave, propagating along the surface of an elastic substrate, whose amplitude decays exponentially with substrate depth.

Surface Acoustic Wave Device

Passive circuit element using surface acoustic waves. The main applications are as bandpass filters and as delay lines.

* Definition from: Surface acoustic wave filters. International Standard. Bureau Central de la Commision Electrotechnique Internationale, CEI IEC 862-1. 1989.

IMAGE EVALUATION TEST TARGET (QA-3)

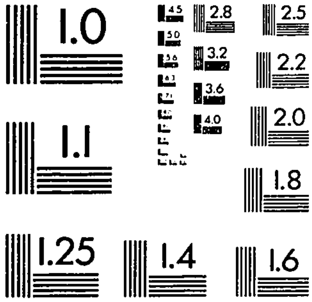

150mm

6″

APPLIED IMAGE. Inc
1653 East Main Street
Rochester, NY 14609 USA
Phone: 716/482-0300
Fax: 716/288-5989